

Stellar Migration and Chemical Enrichment in the Milky Way

James W. Johnson,¹★ David H. Weinberg,^{1,2} Fiorenzo Vincenzo,² Jonathan C. Bird,³ Sarah R. Loebman,⁴ Alyson Brooks,⁵ Thomas R. Quinn,⁶ Charlotte R. Christensen,⁷ et al.?

¹ Department of Astronomy, The Ohio State University, 140 W. 18th Ave., Columbus, OH, 43210, USA

² Center for Cosmology and Astroparticle Physics (CCAPP), The Ohio State University, 191 W. Woodruff Ave, Columbus, OH, 43210, USA

³ Department of Physics & Astronomy, Vanderbilt University, 2301 Vanderbilt Place, Nashville, TN, 37235, USA

⁴ Department of Physics, University of California Merced, 5200 North Lake Rd., Merced, CA, 95343, USA

⁵ Department of Physics & Astronomy, Rutgers University, 136 Frelinghuysen Rd, Piscataway, NJ, 08854, USA

⁶ Department of Astronomy, University of Washington, Box 351580, Seattle, WA, 98195, USA

⁷ Department of Physics, Grinnell College, 1116 8th Ave., Grinnell, IA, 50112, USA

Accepted XXX; Received YYY; in original form ZZZ

ABSTRACT

We investigate the impact of stellar migration on galactic chemical evolution models, considering a handful of assumptions for the star formation history and time-dependence of radial migration based on a zoom-in, hydrodynamical N-body simulation of galaxy evolution. To this end, we extend the *Versatile Integrator for Chemical Evolution* (VICE), developing and making use of its `milkyway` object, built to handle these models under a wide variety of assumptions. We find that models for the time-dependence of radial migration impact the type Ia supernova rate as a function of both time and radius, inducing significant variability. We demonstrate that this is a means with which young, α -enhanced stars can arise naturally out of inside-out galaxy growth with stellar migration. We find that the observed age-[α /Fe] relation is well-fit by an inside-out star formation history, while the age-[O/H] and age-[Fe/H] relations are well-fit by a late starburst model; no one model investigated here fits both simultaneously. Lastly, we find that none of our models predict an [α /Fe] dichotomy resembling that observed in the Milky Way. This suggests that inside-out galaxy growth combined with radial migration, even with a late starburst, is not conducive to forming the infamous bimodality. We postulate that more dramatic evolutionary events (e.g. a two-infall model) are necessary to describe the observed results. VICE is publicly available at <https://pypi.org/project/vice>.

Key words: methods: numerical – galaxies: abundances, evolution, star formation, stellar content

1 INTRODUCTION

- The Age-Metallicity Relation (AMR)

– Known for some time that stars undergo radial migration, but to date there are only a handful of chemical evolution models that take this into account (Wielen et al. 1996; Edvardsson et al. 1993; Sellwood & Binney 2002; Schönrich & Binney 2009; Minchev et al. 2013, 2014, 2017; Sharma et al. 2020).

– Age-metallicity relation in the solar neighbourhood exhibits considerable intrinsic scatter (Edvardsson et al. 1993), usually attributed to radial migration of metal-rich (metal-poor) stars formed at smaller (larger) Galactocentric radii (Sellwood & Binney 2002; Haywood 2008; Roškar et al. 2008b; Schönrich & Binney 2009).

– Feuillet et al. (2018) reveal that super-solar metallicity stars are statistically older than solar metallicity stars (their Fig. 3). Contrasts with simple one-zone models where enrichment proceeds alongside star formation yielding a monotonic AMR (e.g. Andrews et al. 2017; Weinberg et al. 2017). One-zone models of starbursts can produce non-monotonic AMR due to the effect of dilution (Johnson & Weinberg 2020), but they by construction do not predict multiple abundances at fixed age.

- The Young Alpha-Rich Population

– Population of young (~few Gyr), [α /Fe] \sim 0.1–0.2 stars in the solar neighbourhood.

– Found using stellar ages estimated carbon-to-nitrogen ratios (Martig et al. 2016), isochrone matching (Feuillet et al. 2018, 2019), and with the asteroseismic ages in the original APOKASC catalog (Silva Aguirre et al. 2018; Pinsonneault et al. 2014).

– Mor et al. (2019) infer a factor of \sim 2 enhancement in the

* Contanct e-mail: johnson.7419@osu.edu

SFH of the Milky Way ~ 2 Gyr ago by comparing population synthesis models to observed stellar luminosity functions and color-magnitude diagrams from Gaia data (Gaia Collaboration et al. 2018). Isern (2019) reach similar conclusions by modeling the white dwarf luminosity function in the solar neighbourhood with Gaia parallaxes. Motivated by these results, Johnson & Weinberg (2020) demonstrate using one-zone chemical evolution models that a recent starburst can produce young, α -enhanced stars. Caveat: burst would have had to be sufficiently localized such that the young, α -rich stars remain outliers from an otherwise monotonically decreasing age-[α /Fe] relation.

- The [α /Fe] bimodality

- Milky Way stars segregate themselves into the low- and high- α sequences, a bimodality found in, e.g., Gaia ESO (Recio-Blanco et al. 2014; Rojas-Arriagada et al. 2017), and APOGEE (Nidever et al. 2014; Hayden et al. 2015; Weinberg et al. 2019).

- Presence is well established, though origin a topic of intense debate.

- Notion that it could arise out of radial migration traces back to Schönrich & Binney (2009).

- Weinberg et al. (2017) models suggest increase in strength of the mass-loading factor η at late times would lower the equilibrium abundance, forming stars along the low- α sequence. This plus radial migration is yet unexplored.

- Spitoni et al. (2019) demonstrate that two-infall models can reproduce solar annulus data with good agreement. This plus radial migration is yet unexplored.

- Grand et al. (2018) find with Auriga (Grand et al. 2017) that early, accretion induced starburst populates the high- α sequence, followed by low-level, sustained star formation on low- α sequence, and a rapid transition between the two ensures chemical space relatively unpopulated. This would imply short τ_\star (see justification in Weinberg et al. 2017). Ongoing, low-metallicity gas accretion can also populate low- α sequence. Buck (2020) find results qualitatively similar to second scenario in NIHAO simulation suite (Wang et al. 2015; Buck et al. 2020). Hydrodynamical simulations take into account radial migration by construction.

- Clarke et al. (2019) show that star formation proceeded in clumps in an SPH simulation of an NFW halo using GASOLINE (Navarro et al. 1997; Wadsley et al. 2017). The clumps self-enrich, forming stars on the high- α sequence, while more spatially extended, smooth star formation populated the low- α sequence.

- No shortage of models that reproduce the dichotomy, yet only those done with hydrodynamical simulations and a handful of others have taken into account radial migration.

2 DATA AND METHODS

- This paper is meant to address the simple question of: “When combining simple, realistic assumptions about the star formation and dynamical histories of the Milky Way, what observed results can be replicated?”

2.1 Multi-Zone models

- Multizone models are a means of extending traditional one-zone models to take into account the motions of stars and gas by allowing the exchange of both between zones.

- Qualitatively similar approach in Matteucci & Francois (1989); Schönrich & Binney (2009); Minchev et al. (2013).

- VICE released in Johnson & Weinberg (2020), presented first results from `singlezone` object. Develop the `multizone` object and the `milkyway` extension of that, and make use of them here. `multizone` simply provides an array of `singlezone` objects and allows the exchange of gas and individual stellar populations between any two zones at any given simulation time. `milkyway` forces an annular model, where here we take a width of 100 pc, and adopts by default the migration scheme discussed in the next subsection.

- Don’t go into gory detail here, but provide a brief summary of VICE’s algorithm. Further details can be found in the science documentation.

- At its core, the `multizone` object is an array of `singlezone` objects, each with its own ISM mass, star formation rate, and infall rate. `multizone` migration prescriptions describe how gas and stars move between zones. Gas can be moved between any pair of zones according to user-constructed functions of time. Stars are stand-ins for entire stellar populations, and the user has full control over what zone every single stellar population is in at every single timestep. This should allow arbitrarily complex zone schema to be implemented. Hydrodynamical simulations form varying numbers of star particles of fixed mass, but VICE forms a fixed number of stellar populations per zone per timestep, each with a mass that is simply $\dot{M}_\star \Delta t / n$ where \dot{M}_\star is the star formation rate, Δt is the timestep size, and n is the number of stellar populations per zone per timestep.

- `milkyway` object extends the `multizone` object and assumes an annular zone configuration, automatically adopting the migration schema from this paper as a default. There is thus a fixed number of stellar populations per annulus per timestep.

2.2 Radial Migration

- Algorithm based on initial and final radii of star particles in hydrodynamical simulations.

- Stellar populations assumed to be born at centres of their annuli. For a stellar population born at time T and Galactocentric radius R_{gal} , VICE searches for star particles formed at $T \pm 300$ Myr and $R_{\text{gal}} \pm 250$ pc. It then randomly selects a star particle from this subsample with no bias to act as an *analog*. Adopts the final radius of the star particle at face value, and moves from its radius of birth to the final radius at $T = 12.7$ Gyr with some time dependence. If no candidate analogs are found, search is widened to $T \pm 600$ Myr and $R_{\text{gal}} \pm 500$ pc. If still no candidate analogs are found in this widened search, the stellar population is assumed to remain at its birth radius and to have a final height above the disk midplane of $z = 100$ kpc. These stellar populations are few in number.

- We have zones only for each annulus from $R_{\text{gal}} = 0$ to 20 kpc; there are no zones off the midplane, retaining the assumption that the gas-phase abundances are vertically well mixed as well as azimuthally. Each stellar population simply assumes the final height $|z|$ of its assigned analog, though this doesn’t enter into the simulations at all; it’s purely post-processing information.

- When a star particle is assigned as an analog to a stellar population in our simulations, it is *not* thrown out of the sample of candidate analogs, allowing star particles to in theory act as analogs for multiple stellar populations. This is a difference between the Minchev et al. (2013) model and ours.

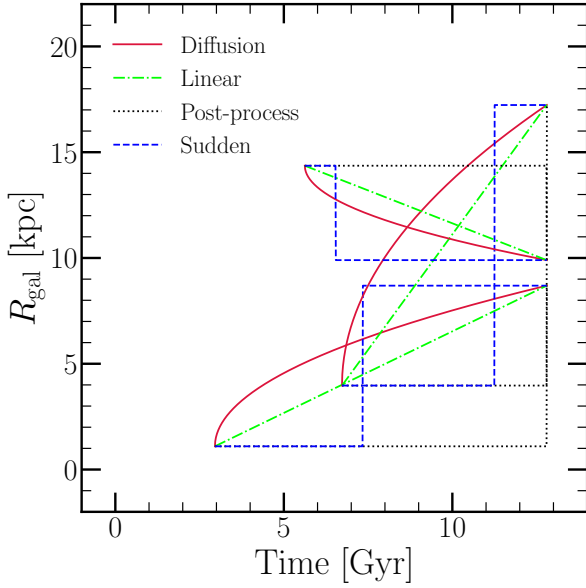


Figure 1. A diagram illustrating how Galactocentric radius changes with time for three stellar populations under our migration schema: diffusion (crimson, solid), linear (lime, dot-dashed), post-process (black, dotted), and sudden (blue, dashed). Here the initial and final radii and birth times are pseudorandom numbers drawn from a uniform distribution for illustrative purposes. With the initial and final Galactocentric radii of a stellar population, its birth time, and one of these assumptions about the time-dependence of migration, the Galactocentric radius at all times is known.

- Our migration models

- All neglect radial gas flows, this paper instead focusing on four simple models for how the radius of a stellar population’s orbit changes with time. Investigation of our models with radial gas flows would be an interesting extension to this paper.

- **Post-processing:** Stars stay where they are born until the final timestep. Based on the assumption that stellar populations do not contribute to enrichment beyond their birth radius (e.g. Minchev et al. 2013). Each annulus simulated as a one-zone model independent of all other zones. Shown in black dotted line in Fig. 1.

- **Sudden:** A random number is drawn from a uniform distribution between the time of birth and the present day. That time is taken to be the time of instantaneous migration of the present-day annulus. Emulates a scenario in which a single dynamical interaction changes the orbital radius of a star. Can be thought of as a time-dependent extension of the post-processing scenario. Shown in blue dashed line in Fig. 1.

- **Diffusion:** Continuous, time-dependent migration with a \sqrt{t} dependence. Emulates a scenario in which angular momentum diffuses throughout the disk via a random walk, in which case the mean displacement of a star from its birth radius would scale with \sqrt{t} . Shown in red solid line in Fig. 1.

- **Linear:** A simple time-dependent variation of the diffusion model. Has no physical motivation other than numerical ease, but together with the diffusion model constitutes a test of how sensitive our models are to the assumed time-dependence of radial migration. Demonstrated by green dot-dashed line in Fig. 1.

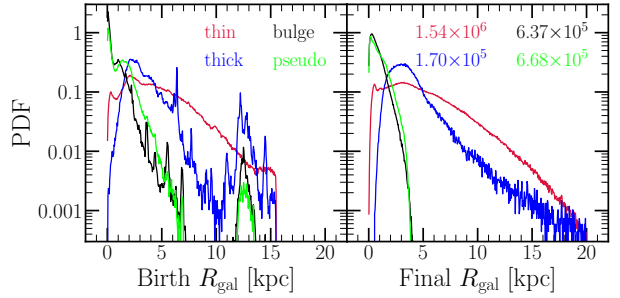


Figure 2. Distributions of h277 star particles in their birth (left) and final (right) Galactocentric radii. Distributions are shown for thin disk (crimson), thick disk (blue), bulge (black), and pseudobulge (lime) populations according to the kinematic decomposition described in § X. In the right-hand panel we denote the number of star particles in each population according to the same color-coding. I cut off R_{Form} at 15.5 kpc in my reduction from Jon’s file of star particles. Extend it to 20 kpc, just for the sake of having candidate analogs out there for future papers? We can still cut off star formation here at 15.5 kpc, so any stars that form out there and migrate inward will have zero mass and thus no effect, but maybe worth it for showing the distributions. I’d only have to change one line of code and rerun things.

2.3 The Hydrodynamical Simulation

- In this paper we take h277 (Christensen et al. 2012; Zolotov et al. 2012; Loebman et al. 2012, 2014; Brooks & Zolotov 2014). Its data and our migration schema are built directly into VICE’s `milkyway` object as defaults for ease of use. A synopsis of the simulation parameters can be found in § 2 of Bird et al. (2020).

- Find that h277 has only a small fraction of star particles born in the first 1 Gyr of its 13.7 Gyr run, so $T = 1$ Gyr is a much better estimate of the onset of star formation than $T = 0$ Gyr. Chop off the star particles born in the first Gyr of evolution, and subtract 1 Gyr from their formation times, thus running disk models for 12.7 Gyr.

- Of particular importance to have accurately measured formation radii for each star particle that we use as candidate analogs as discussed in § 2.2. h277 did not record the exact birth radius of each star particle; however, each star particle does have an accurate age at each snapshot. Therefore, one has a reasonable approximation of the birth radius of each star particle that is sufficiently young in the first snapshot in which it was recorded. Therefore, we restrict our sample of candidate analogs to those with an age at first snapshot of ≤ 150 Myr, and adopt their Galactocentric radius at first snapshot as the birth radius. Also conducted the analysis with age at first snapshot of ≤ 50 Myr, and found similar results, suggesting this choice does not impact our conclusions. In practice find that 150 Myr also provides us with an adequately large number of star particles to sample analogs from, such that our predicted abundance distributions in various Galactic regions are not limited by stellar population counts (in particular far off the plane).

- Excluding halo stars, but including bulge, pseudobulge, and thin- and thick-disk stars yields sample of 3,019,521 candidate analog star particles. Included those because it’s likely the majority formed within a reasonably spatially confined region around the disk, suggesting they contributed at least in part to its chemical evolution. **Expand on this:** disk stars are only about 45% of the total sample, so our simulations run with ~ 1.5 million stellar populations with assigned analogs to avoid oversampling. Plot distributions of initial and final radii.

- Can be thought of as adopting the dynamical history of h277 in

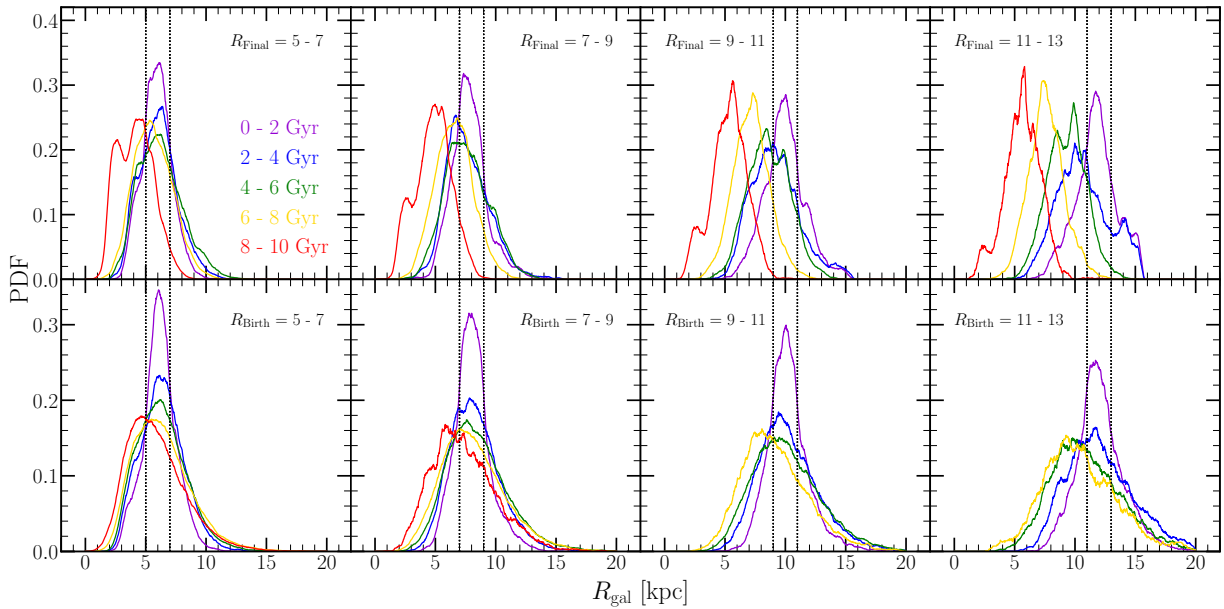


Figure 3. Radial distributions of our candidate analog star particles from h277. In the top row, we show distributions of *birth* radius in bins of final radius and age. In the bottom row, we show distributions of *final* radius in bins of birth radius and age. Each bin in Galactocentric radius is shown in its own panel, denoted in text at the top of the panels and by vertical black dashed lines. We color-code the distributions according to the age of the star particles and the legend in the upper left panel. We smooth all distributions with a box-car width of 0.5 kpc to improve clarity. We omit the distributions for 8 - 10 Gyr old stars born in the 9 - 11 and 11 - 13 kpc bins due to an insufficient number of star particles with which to calculate the distribution.

our disk models. Advantage to this approach is that we get a migration model with no free parameteres. Minchev et al. (2013) adopts similar approach with a hydrodynamical simulation, but did not investigate time-dependent migration. Schönrich & Binney (2009) did investigate time-dependent migration, though their algorithm was based on dynamical arguments rather than a hydrodynamical simulation, and required fitting to observed data, for which they employed the Geneva-Copenhagen Survey of solar neighbourhood stars (Nordström et al. 2004a; Holmberg et al. 2007). We’re unaware of any studies to date which employ a hydrodynamical simulation to drive radial migration while simultaneously allowing stars to contribute to enrichment beyond their birth radius.

- h277 had a transient bar during its evolution, but does not have a bar at $z = 0$. This could mean that the star particles in h277 migrated in a manner which does not reflect the dynamical history of the Milky Way, but at present inferring a star’s birth radius observationally is notoriously difficult anyway ([citation needed](#)), so its likely the impact of this decision is within current observational uncertainties. Nonetheless, it is worth noting that the Minchev et al. (2013) model, and by extension the Minchev et al. (2014) and Minchev et al. (2017) models as well, selected a hydrodynamical simulation specifically so that it would have a bar at $z = 0$. A detailed investigation of the impact of bar evolution on radial migration and thus chemical evolution is outside the scope of this paper, though can be conducted by simply swapping the birth times and initial and final radii of h277 within VICE and rerunning the simulations.

- Distributions of birth radii in bins of final radii and age are shown in the top row of Fig. 3. Conversely, the bottom row shows distributions of final radii in bins of birth radii and age.

- Focusing on the top row of panels in Fig. 3, we note that the oldest stars at any Galactocentric radius at the present day were overwhelmingly born at smaller radii. The youngest stars, however, were overwhelmingly born at that radius, and the stars

of intermediate ages simply span the range in radii between the two. With increasing radius, the differences in the mode of the birth radius distribution between age bins gets larger.

- Focusing on the bottom row of panels in Fig. 3, we note that for stars born at any radius and time, the distribution of final radii is still peaked near the birth radius. With increasing age, it appears the mode final radius may move slightly inward. The tails of the distributions to large radii are relatively age-independent - some differences between the 0 - 2 and 8 - 10 Gyr age bins, but not much. However, the tails of the distributions to small radii are not age-independent, and move toward smaller R_{gal} with increasing age. This suggests that radial migration inward and outward occur on different timescales, in particular that inward migration occurs on longer timescales than outward migration. By extension this may suggest that inward and outward migration are tied to different physical processes. Roškar et al. (2008a) demonstrate using a cosmological simulation that resonant scattering at corotation causes stars to move outward and gas to move inward. It’s possible that radial migration inward is has different origins.

- The differences in distributions shown in the top and bottom panels boils down to stellar surface density being a strong function of Galactocentric radius. Take for example the age = 8 - 10 Gyr bin in both $R_{\text{Birth}} = 5 - 7$ kpc and $R_{\text{Final}} = 11 - 13$ kpc bins (i.e. the red curves in the bottom-left and top-right panels). For these old stars born at 5 - 7 kpc, 11 - 13 kpc is far down the tail of the R_{Final} distribution, and yet 5 - 7 kpc is the mode R_{Birth} of all old stars presently at these radii. This is only possible if the stellar surface density gradient is sufficiently steep, which it is known to be (e.g. Bland-Hawthorn & Gerhard 2016).

- Fig. 3 also demonstrates that the numbers of stars that migrated inward and outward are comparable in h277. Taking a $|\Delta R_{\text{gal}}| \geq 500$ pc between birth and final radii as the criterion for migrating inward or outward, indeed we find that in

our sample of candidate analogs, 27% migrated inward, 29% migrated outward, and the remaining 44% stayed near their birth radius.

– In all bins of birth radius, a good first-order estimate of the probability density that a star has a final radius in the same bin is $\sim 0.2 - 0.3$. With bins in radius on this plot of 2 kpc, that suggests that 40 - 60% of stars migrate significantly beyond their birth radius by the time they’re ~ 2 Gyr old. If the SN Ia DTD is a $t^{-1.1}$ power-law as suggested by recent observations (e.g. Maoz & Mannucci 2012; Maoz & Graur 2017), then we expect similar numbers of SN Ia events to occur with delay times between 1 and 10 Gyr as we do between 100 Myr and 1 Gyr. With such an extended DTD, and the distributions in final radius shown in the bottom panel of Fig. 3, its possible that white dwarfs migrate significant distances before producing a SN Ia event. This is the motivation for our test of whether or not the radial migration of nucleosynthetic yields is a statistically significant effect.

2.4 Nucleosynthetic Yields

- Brief background on VICE’s algorithm: we form a given number of stellar populations in each zone and at each timestep. They then migrate between zones according to our algorithm and eject CCSN and SN Ia products as smooth functions of time according to our yields.

- *Fractional net* yields, as required by VICE.
- Take our yields from Weinberg et al. (2017) and Johnson & Weinberg (2020). Find that our models with these yields predict $[O/Fe] \approx +0.05$ for zero age stars, so we multiply SN Ia Fe yield by $10^{0.1}$ to produce more realistic late-time $[O/Fe]$. This is likely within the uncertainties in nucleosynthetic yields.
- CCSN products injected immediately, and thus unaffected by migration:

$$\dot{M}_x^{\text{CC}} = y_x^{\text{CC}} \dot{M}_{\star} \quad (1)$$

- SN Ia products injected with a $t^{-1.1}$ DTD, with minimum delay $t_D = 150$ Myr.

$$\dot{M}_x^{\text{Ia}} = y_x^{\text{Ia}} \sum_i M_i R_{\text{Ia}}(\tau_i) \quad (2)$$

where the summation is taken over all stellar populations in a given zone, and M_i and τ_i denote the mass and age of the i ’th stellar population in a given zone at a given time. The SN Ia rate R_{Ia} is normalized such that the integral over the time interval from t_D to a maximum time of 15 Gyr is equal to one.

- We include AGB star enrichment according to the FRUITY database net yields (Cristallo et al. 2011), though these yields are not significant compared to the CCSN and SN Ia yields for O and Fe. Our results can be interpreted as if they were zero. Algorithm is based on calculating the mass in dying stars from previously formed stellar populations at each timestep, details can be found in Johnson & Weinberg (2020) and in VICE’s science documentation¹.
- Minchev et al. (2013) adopt much lower nucleosynthetic yields, because they don’t have outflows. Discuss differences in how we obtain the late-time metallicity gradient either here or at the end of § 2.5.

¹ https://vice-astro.readthedocs.io/en/latest/science_documentation/enrichment/index.html

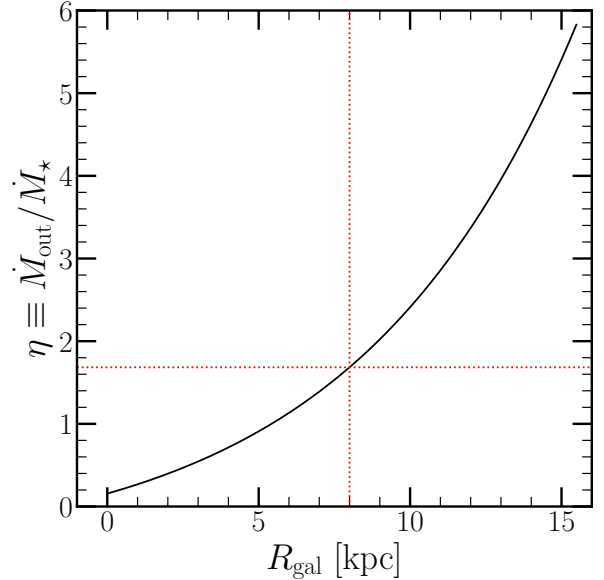


Figure 4. Our implemented scaling of the mass loading factor η with Galactocentric radius (black) as defined by equation (5). The horizontal and vertical red dashed lines highlight the value of $\eta \approx 1.7$ at an assumed orbital radius of the sun of $R_{\odot} = 8$ kpc.

2.5 Outflows

- $\eta \equiv \dot{M}_{\text{out}}/\dot{M}_{\star}$
- Implement a scaling of η with R_{gal} such that a realistic metallicity gradient is produced at late times. A fundamental observable, the observed metallicity gradient in the Milky Way has been the focus of a considerable number of studies to date.
 - Nordström et al. (2004b) find a gradient of -0.099 kpc^{-1} in $[\text{Fe}/\text{H}]$ in main sequence stars from GCS (Nordström et al. 2004a; Holmberg et al. 2007).
 - Daflon et al. (2009) find a gradient of -0.04 kpc^{-1} in $[\text{S}/\text{H}]$ in OB stars
 - Frinchaboy et al. (2013) find a gradient of -0.09 kpc^{-1} in $[\text{M}/\text{H}]$ in open clusters.
 - Hayden et al. (2014) also find -0.09 kpc^{-1} in $[\text{M}/\text{H}]$ for $R_{\text{gal}} \gtrsim 6$ kpc for low- α stars. For $R_{\text{gal}} \lesssim 6$ kpc, they find a relatively flat gradient.
 - Weinberg et al. (2019) finds -0.06 kpc^{-1} in mode($[\text{Mg}/\text{H}]$) for upper red giant branch disk stars (see their Fig. 23).

- The procedure outlined in this section reproduces the metallicity gradient while neglecting the impact of radial migration. We demonstrate in § 3.2 that this assumption holds in our simulation outputs which do take it into account.
 - Our recipe for ensuring a reasonable gradient hinges on the assumption that the mode $[\text{X}/\text{H}]$ for any given element x at any given radius R_{gal} reflects the equilibrium abundance of that element at that radius.
 - For α elements, Weinberg et al. (2017) defines the equilibrium abundance under a constant SFH as:

$$Z_{\alpha,\text{eq}} = \frac{y_{\alpha}^{\text{CC}}}{1 + \eta(R_{\text{gal}}) - r} \quad (3)$$

where η is the mass-loading factor at that radius R_{gal} , and r is the recycling parameter (≈ 0.4 for the sake of this scaling with a Kroupa

IMF; Weinberg et al. 2017). Solving for $\eta(R_{\text{gal}})$ yields:

$$\eta(R_{\text{gal}}) = \frac{y_{\alpha}^{\text{CC}}}{Z_{\alpha,\text{eq}}} + r - 1 = \frac{y_{\alpha}^{\text{CC}}}{Z_{\alpha,\odot}} 10^{-\text{mode}([\text{X/H}](R_{\text{gal}}))} + r - 1 \quad (4)$$

- We assume a slope of -0.08 kpc^{-1} , in tentative agreement with the previous studies that quote the slope of the gradient mentioned above. To set the normalization, we assume the mode([X/H]) to be $\sim +0.3$ at $R_{\text{gal}} = 4 \text{ kpc}$, since this would produce $\text{mode}([\text{X/H}]) \approx 0$ at $R_{\text{gal}} \approx 7 - 9 \text{ kpc}$. This results in the following form for η as a function of Galactocentric radius:

$$\eta(R_{\text{gal}}) = \frac{y_{\alpha}^{\text{CC}}}{Z_{\alpha,\odot}} 10^{(-0.08 \text{ kpc}^{-1})(R_{\text{gal}} - 4 \text{ kpc}) + 0.3} + r - 1 \quad (5)$$

- This does assume a uniformly linear gradient at all R_{gal} . Hayden et al. (2014) do find the gradient in [M/H] to flatten for $R_{\text{gal}} \lesssim 6 \text{ kpc}$, challenging this assumption. However, this procedure can be easily repeated for any desired gradient, since the functional form simply goes into the power of 10 in equation (5).

- Model based on assumption that observed mode([α/H]) as a function of Galactocentric radius reflects the equilibrium α abundance at each radius (i.e. $\text{mode}([\alpha/\text{H}]) = \log_{10}(Z_{\alpha,\text{eq}}/Z_{\alpha,\odot})$)

- We adopt our yield of O for y_{α}^{CC} and the solar abundance of O of $Z_{\text{O},\odot} = 0.00572$ from Asplund et al. (2009).

- Fig. 4 plots this scaling of η with R_{gal} , highlighting the value for the solar circle.

- Minchev et al. (2013) did not include outflows in their model, and as such have much lower yields. Discuss differences in how we obtain the late-time metallicity gradient either here or at the end of § 2.4.

2.6 Recycling

- As mentioned in § 2.4, we’re using *net* rather than *gross* yields. Our yields thus only quantify the amount of *newly produced* metals from each stellar population, and the return of previously produced material must be taken into account.
- Weinberg et al. (2017) defined the *cumulative return fraction* r to be the fraction of a single stellar population’s initial mass that has been returned to the ISM. In detail, r is a complicated function of the age of a stellar population τ which depends on the assumptions about stellar lifetimes, the IMF, and an initial-remnant mass relation (e.g. Kalirai et al. 2008).

– Weinberg et al. (2017) demonstrated that the assumption of *instantaneous recycling* is a reasonable approximation, where instantaneous recycling refers only to previously produced material, contrary to what most people mean when they refer to instantaneous recycling. They show that $r = 0.4$ (0.2) is a good approximation for a Kroupa (Salpeter) IMF. However, this was demonstrated for smooth star formation histories and in parameter spaces conducive to analytic solution. Because numerical integration of $r(\tau)$ is neither challenging nor time-consuming, VICE by default implements continuous recycling by solving $r(\tau)$ at the beginning of each simulation given the IMF, the Kalirai et al. (2008) initial-remnant mass model, and the assumption that $\tau = \tau_{\odot}(M/M_{\odot})^{-3.5}$. We also assume a post-main sequence lifetime of 10% of the main sequence lifetime for all stars.

- The detailed form the recycling rate in a given annulus and at a given time is:

$$\dot{M}_x^r = \sum_i Z_{x,i} M_i \dot{r}(\tau_i) \quad (6)$$

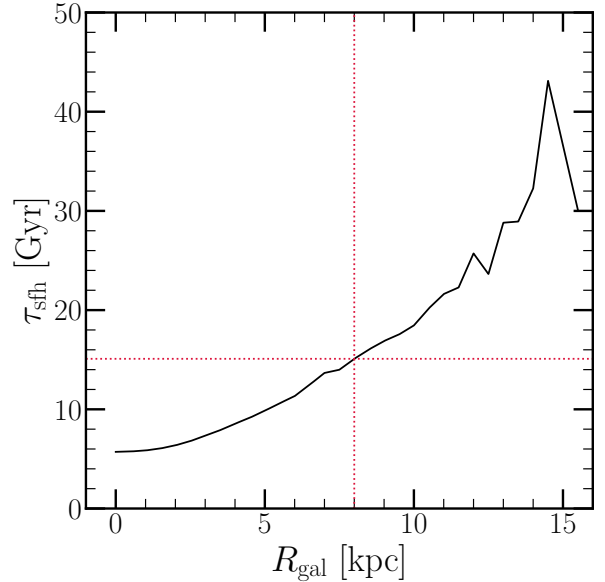


Figure 5. The e-folding timescales of star formation as reported by Sánchez (2020) for $10^{10.5} - 10^{11} M_{\odot}$ Sa/Sb Hubble type galaxies (black), assuming a half-light radius of $R_e = 5 \text{ kpc}$ and the mathematical form of our inside-out SFH (see equation (9)). The red dotted lines highlight $\tau_{\text{sfh}} \approx 15 \text{ Gyr}$ at an assumed radius of $R_{\odot} = 8 \text{ kpc}$.

where M_i is the mass of the i ’th stellar population in the annulus, τ_i is its age, $Z_{x,i}$ is its birth abundance of some element x , and the summation is taken over all stellar populations in the annulus at that time.

- We implement continuous recycling in our simulations, but at a number of places in analyzing their results here, we adopt the instantaneous approximation for ease.

2.7 Star Formation Histories

- Appendix A presents justification of how we normalize our parameters to produce a realistic Milky Way at the end of the simulation. In short, it takes in a unitless description of the time-dependence of the SFH at a given Galactocentric radius, denoted $f(t|R_{\text{gal}})$, and a unitless description of the radial dependence of the present-day stellar surface density, denoted $g(R_{\text{gal}})$. Neglecting radial migration, it then integrates $f(t|R_{\text{gal}})$ at each radius with time and $g(R_{\text{gal}})$ over the area of the disk to ensure that the correct present-day stellar mass and desired surface density gradient Σ_{\star} are produced by the simulation. This recipe hinges on the assumption that radial migration does not significantly alter the form of Σ_{\star} , which we demonstrate in § 3.1 to be the case under our model and for h277’s dynamical history. As long as this assumption isn’t violated, this recipe can be used.

- Adopt the Licquia & Newman (2015) total stellar mass of $(6.08 \pm 1.14) \times 10^{10} M_{\odot}$. We’re including bulge star particles in our sample of candidate analogs from h277, so we model the entire stellar mass as opposed to just the disk, for which Licquia & Newman (2015) found $(5.17 \pm 1.11) \times 10^{10} M_{\odot}$.

- Take the gradient from Bland-Hawthorn & Gerhard (2016), which characterize the disk as a double exponential - the sum of two single exponentials representing the thin and thick disks. This

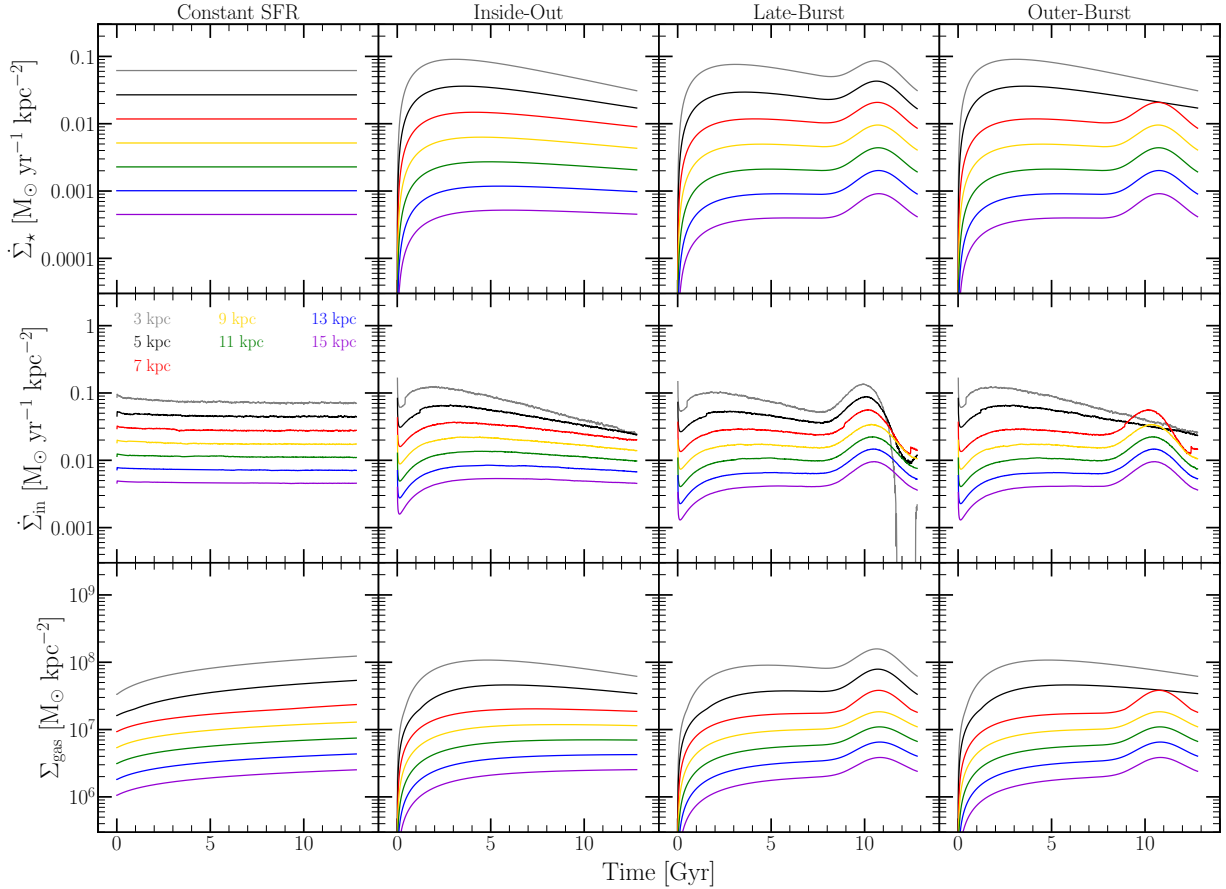


Figure 6. The surface densities of star formation $\dot{\Sigma}_\star$ (top row), infall $\dot{\Sigma}_{in}$ (middle row), and gas Σ_{gas} (bottom row) as functions of simulation time for our four fiducial SFHs: constant (far left), inside-out (left middle), late-burst (right-middle), and outer-burst (far right). We plot curves for the annuli whose inner radii are 3 kpc (grey), 5 kpc (black), 7 kpc (red), 9 kpc (yellow), 11 kpc (green), 13 kpc (blue), and 15 kpc (purple) (see equations (8), (9), (10), and (11) for the mathematical definition of each SFH).

has the following form:

$$g(R_{gal}) = e^{-R_{gal}/r_t} + \frac{\Sigma_T}{\Sigma_t} e^{-R_{gal}/R_T} \quad (7)$$

where r_t and R_T are the scale radii of the thin and thick disks, respectively, and Σ_T/Σ_t is the ratio of the surface densities to thin and thick disk stars at $R_{gal} = 0$. Based on the results of Bland-Hawthorn & Gerhard (2016), we take in this paper $r_t = 2.5$ kpc, $R_T = 2.0$ kpc, and $\Sigma_T/\Sigma_t = 0.27$.

- We present four fiducial SFHs, which we dub “constant”, “inside-out”, “late-burst”, and “outer-burst”. They’re defined as follows:

– **Constant:** The SFH at a given radius is time-independent.

$$f_C(t|R_{gal}) = 1 \quad (8)$$

This case is of particular theoretical interest because it quantifies the effect of ongoing with star formation with radial migration, and no additional effects.

– **Inside-Out:**

$$f_{IO}(t|R_{gal}) = (1 - e^{-t/\tau_{rise}}) e^{-t/\tau_{sfh}} \quad (9)$$

We adopt this scenario over the traditional linear-times-exponential form of $f(t|R_{gal}) \sim t e^{-t/\tau_{sfh}}$, because the latter does not offer control over the position of the maximum. The

form we adopt has a maximum near τ_{rise} , for which we adopt a value 2 Gyr everywhere in this paper. We find that this produces a peak in star formation at lookback times of ~ 10 Gyr, corresponding to a redshift of $z \approx 2$, which is around cosmic high noon. In this paper τ_{sfh} is a function of R_{gal} here, and we discuss it briefly in a few paragraphs.

– **Late-Burst:** An inside-out SFH with a gaussian describing a starburst.

$$f_{LB}(t|R_{gal}) = f_{IO}(t|R_{gal})(1 + A_b e^{-(t-t_b)^2/2\sigma_b^2}) \quad (10)$$

A_b is a dimensionless parameter describing the strength of the starburst, t_b is the time of the local maximum in the SFH during the burst, and σ_b is the width of the gaussian describing it. Loosely motivated by the findings of Isern (2019) and Mor et al. (2019). Here we take $A_b = 1.5$, $t_b = 10.8$ Gyr, and $\sigma_b = 1$ Gyr.

– **Outer-Burst:** A variation of the late-burst model in which only $R_{gal} \geq 6$ kpc experience the starburst. Loosely motivated by findings of Vincenzo & Kobayashi (2020) where a hydrodynamical simulation of a Milky Way-like galaxy showed radially dependent infall.

$$f_{OB}(t|R_{gal}) = \begin{cases} f_{IO}(t|R_{gal}) & (R_{gal} < 6 \text{ kpc}) \\ f_{LB}(t|R_{gal}) & (R_{gal} \geq 6 \text{ kpc}) \end{cases} \quad (11)$$

- Derive e-folding timescales of star formation τ_{sfh} from the data in Sánchez (2020).

– They present the stellar surface density Σ_\star as a function of age in bins of R/R_e for MaNGA galaxies, where R_e is the half-light radius. They conduct this analysis in bins of stellar mass and for different Hubble types. Here take their $M_\star = 10^{10.5} - 10^{11} M_\odot$ bin for Sa/Sb spirals (i.e. Milky Way-like galaxies).

– With our gradient, we know the present-day half-mass radius to be very near 4 kpc (this is just doing a couple integrals over the area of the disk). The findings of García-Benito et al. (2017) and González Delgado et al. (2014) suggest that half-light radii are marginally larger than half-mass radii. Based on equations (4) of González Delgado et al. (2014) relation the two for circular apertures, we expect our model galaxy to have a half-light radius near 5 kpc. We therefore adopt $R_e = 5$ kpc in calculating τ_{sfh} as a function of radius. **As I understand it, there are some results that suggest this value for the Milky Way as well?**

– Their reported Σ_\star -age relation is not robust enough to get individual SFHs directly, but does allow the parameters of some fiducial mathematical model to be fit to the population-averaged data. Assuming the $f_{\text{fO}}(t|R_{\text{gal}})$ form, we simultaneously fit the normalization and the e-folding timescale τ_{sfh} to these data. Although the normalization is irrelevant to our simulations and determined via the method outlined in Appendix A, we adopt the resulting $\tau_{\text{sfh}}-R_{\text{gal}}$ relation in our models. Results are shown in Fig. 5.

– Note that the star formation timescales are long, even for the solar annulus ($\tau_{\text{sfh}} \approx 15$ Gyr at $R_\odot = 8$ kpc) and especially for the outer galaxy. Beyond the solar annulus, SFHs are nearly constant after the initial rise at early times.

- Given the assumed star formation histories, the gas supply at all times is known via the SFE timescale τ_\star (discussed in § 2.8). With the amount of gas lost to star formation and outflows at each timestep, the infall rate is also known at all timesteps. The results of all three are shown in Fig. 6.

2.8 Star Formation Efficiency

- The term “star formation efficiency” (SFE) is an overloaded term in the literature. In the star formation/ISM literature, it usually refers to the fraction of a molecular cloud’s mass which will eventually be converted into stars. In the chemical evolution literature, however, it usually refers to the inverse timescale relating the star formation rate within some gas reservoir and the mass of the gas reservoir itself: $\tau_\star \equiv M_{\text{gas}}/\dot{M}_\star$. High (Low) values of τ_\star indicate slow (fast) star formation and thus low (high) SFE; when we refer to SFE here, we’re referring to the definition based on this timescale.

– Potentially note that this is often referred to as the “depletion time” in the ISM literature, and the Weinberg et al. (2017) definition of depletion time: $\tau_{\text{dep}} \equiv \tau_\star/(1 + \eta - r)$.

– In our models, τ_\star increases with decreasing molecular fraction: $\tau_\star = \tau_\star^{\text{mol}}/f_{\text{mol}}$, where τ_\star^{mol} is the same parameter, but for gas that is entirely H_2 . We let it bottom out at this value because it’s believed that star formation proceeds in the molecular phase, although there is significant scatter in the observed relation (e.g. Leroy et al. 2008; Kennicutt & Evans 2012; Tacconi et al. 2018).

- Here we implement a modified Kennicutt-Schmidt Law (Schmidt 1959, 1963; Kennicutt 1998) to describe the scaling of τ_\star with Σ_g . Below some threshold density $\Sigma_{g,\text{Crit}}$, we adopt a power-law with index $k = 0.5$, based on the $N = 1.5$

power-law describing the $\dot{\Sigma}_\star - \Sigma_g$ relation². Above this threshold, we assume the molecular fraction in the ISM to be unity, and to form stars at the rate determined by τ_\star^{mol} . That is:

$$\tau_\star = \begin{cases} \tau_\star^{\text{mol}} \left(\frac{\Sigma_g}{\Sigma_{g,\text{Crit}}} \right)^k & (\Sigma_g \leq \Sigma_{g,\text{Crit}}) \\ \tau_\star^{\text{mol}} & (\Sigma_g \geq \Sigma_{g,\text{Crit}}) \end{cases} \quad (12)$$

It’s common in the chemical evolution literature to adopt a pure power-law scaling of τ_\star with Σ_g ; we adopt this alternate form with a minimum value to ensure that the implied τ_\star is never below τ_\star^{mol} at any redshift.

• Observationally, $\Sigma_{g,\text{Crit}}$ is the surface density at which the observed Kennicutt-Schmidt relation switches from quadratic to linear. Bigiel et al. (2008) present observed Kennicutt-Schmidt relations from the HERACLES and BIMA surveys, and Krumholz et al. (2018) presents a compilation of Kennicutt-Schmidt relations observed by Bigiel et al. (2010) and Leroy et al. (2013). Both suggest that the value is at or around $\sim 10 M_\odot \text{ pc}^{-2} = 10^7 M_\odot \text{ kpc}^{-2}$. In practice we find that this predicts a seemingly unrealistically high ISM composition - $f_{\text{mol}} = 1$ for $R_{\text{gal}} \lesssim 6$ kpc, so in this outline we’ve ran our simulations with $\Sigma_{g,\text{Crit}} = 2 \times 10^7 M_\odot \text{ kpc}^{-2}$. However, this did not solve the problem. We’re still debating about what prescription to use here, though the choice makes no difference in our models. It’s likely the final version of this paper will make a simple assumption regarding star formation efficiency, and then demonstrate in Appendix B that the impact is not significant.

• Tacconi et al. (2018) suggest that τ_\star^{mol} should scale with redshift z and the deviation from the star forming main sequence δ_{MS} via $\tau_\star^{\text{mol}} \propto (1+z)^{-0.6} \delta_{\text{MS}}^{-0.44}$. We don’t take into account the effect of δ_{MS} in our models, but we do investigate the redshift dependence. A reasonable approximation to the $t - z$ relation out to $z \approx 3$ is:

$$\frac{t}{t_0} \approx (1+z)^{-5/4} \quad (13)$$

where t_0 is the present-day age of the universe, and t is not simulation time but the age of the universe at any given redshift. Plugging this relation into the Tacconi et al. (2018) scaling yields the following time-dependence for τ_\star^{mol} :

$$\tau_\star^{\text{mol}} = \tau_{\star,0}^{\text{mol}} (t/t_0)^{12/25} \approx \tau_{\star,0}^{\text{mol}} (t/t_0)^{1/2} \quad (14)$$

where $\tau_{\star,0}^{\text{mol}}$ is simply τ_\star^{mol} at the present day. We generalize this formula to the following form:

$$\tau_\star^{\text{mol}} = \tau_{\star,0}^{\text{mol}} (t/t_0)^\beta \quad (15)$$

In this paper we present simulations which adopt $\tau_{\star,0}^{\text{mol}} = 2$ Gyr and $\beta = 1/2$. We have however ran all possible combinations of $\tau_{\star,0}^{\text{mol}} = 1$ and 2 Gyr, $\beta = 0$ and $1/2$, all four of our fiducial SFHs, and all four migration models, a total of 64 simulations. Unless otherwise noted, we find similar results in all dimensions except SFH.

• Fig. 7 shows τ_\star as a function of R_{gal} at six different time stamps predicted by our fiducial models. Wherever τ_\star is at its minimum value is where the ISM is fully molecular.

– From the actual value of τ_\star at a given radius and time and the assumed τ_\star^{mol} in the model, we can derive molecular fractions within the disk. In the models present here, the disk is molecular out to $R_{\text{gal}} \approx 6$ kpc in all models at the present day. The inside-out SFH has a global molecular fraction of $f_{\text{mol}} \approx 84\%$.

² $k = N - 1$ (Johnson & Weinberg 2020).

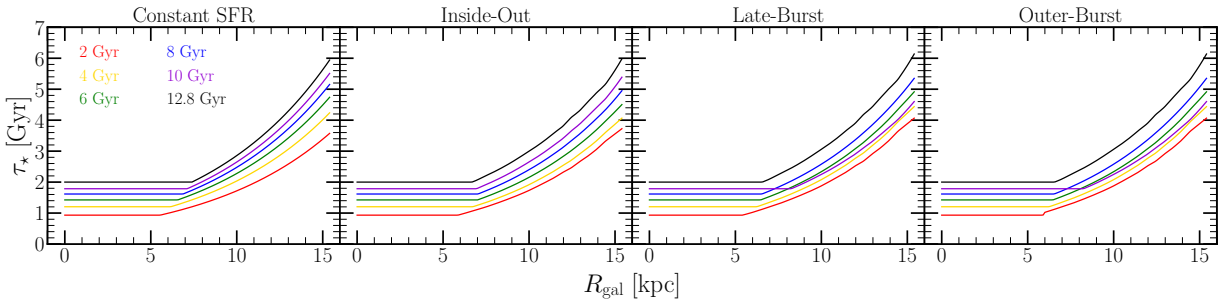


Figure 7. The star formation efficiency (SFE) timescale τ_\star as a function of Galactocentric radius at simulation times of 2 Gyr (red), 4 Gyr (yellow), 6 Gyr (green), 8 Gyr (blue), 10 Gyr (purple), and 12.7 Gyr (i.e. the present day, black) for our four fiducial SFHs: constant (left), inside-out (left-middle), late-burst (right-middle), and outer-burst (right).

2.9 Simulation Parameters

- VICE’s simulations runs in either infall, star formation, or gas mode, referring simply to which one the user is specifying. The fiducial starburst models presented in Johnson & Weinberg (2020) ran in infall mode, but here we run things in star formation mode, since we are after specific forms for the star formation histories of our models.

- We have a sample of 3,019,521 candidate analog star particles from h277, only $\sim 57\%$ of which are disk stars. Since we’re modeling the thin and thick disk populations here, ~ 1.72 million is a much better estimate of the number of analogs that we can realistically sample from. We let star formation extend out to 15.5 kpc, beyond which we force the star formation rate to zero at all times. VICE does form stellar populations at all timesteps in the annuli; they simply have zero mass and thus do not contribute to the chemical evolution or recycling, though they contribute to the computational overhead. With 200 zones and 1,271 timesteps, we let VICE form $n = 8$ stellar populations per zone per timestep, resulting in 2,033,600 stellar populations with predicted masses and abundances, 1,565,872 of which form between $R_{\text{gal}} = 0$ and 15.5 kpc, reasonably within the limit of what we can sample. These simulations run in ~ 2 hours and take up ~ 235 MB per output, including the extra data that we record for each stellar population’s analog star particle.

- To ensure that resolution does not affect our results, we ran the same set of models with $n = 2$ stellar populations per zone per timestep, and found similar predictions.

2.10 The Observed Sample

- For the age-metallicity and age-[α /Fe] relations, we compare to the results of Feuillet et al. (2019). Also compared to Feuillet et al. (2018), the primary difference being that solar metallicity stars are found to be considerably younger in the earlier study.

- I pulled some of this information from David’s two-process paper, which used DR14. Let me know if any of the details of APOGEE and the data reduction have changed since then. Compare metallicity distribution functions to the 16th data release (DR16; Ahumada et al. 2020) of the Apache Point Observatory Galaxy Evolution Experiment (APOGEE; Majewski et al. 2017). A part of the Sloan Digital Sky Survey (SDSS), APOGEE data is collected with a 300-fiber H-band spectrograph (Wilson et al. 2019) on the 2.5-meter Sloan Foundation telescope at Apache Point Observatory (Gunn et al. 2006). The APOGEE sample largely consists of evolved stars with 2MASS (Skrutskie et al. 2006) magnitudes in the range $7 < H < 13.8$ sampled on a grid of sightlines at Galactic latitudes $b = -8^\circ$,

$-4^\circ, 0^\circ, +4^\circ$, and $+8^\circ$ and a wide range of longitudes. Nidever et al. (2015) describes the data processing pipeline for APOGEE, providing the input to the APOGEE Stellar Parameters and Chemical Abundances Pipeline (ASPCAP; Holtzman et al. 2015; García Pérez et al. 2016). ASPCAP simultaneously fits elemental abundances, effective temperatures, and surface gravities using a grid of synthetic spectra predicted by 1-dimensional stellar atmospheric models assuming local thermodynamic equilibrium (Mészáros et al. 2012; Zamora et al. 2015) and the spectral line list provided in (Shetrone et al. 2015). (1-D LTE correct?)

- While we make use of DR16 in comparing our predicted MDFs to the APOGEE data, Feuillet et al. (2018) and Feuillet et al. (2019) made use of the 14th data release (DR14; Abolfathi et al. 2018). We don’t expect this slight difference to impact our conclusions.

3 GRADIENTS

3.1 Surface Density

- SFH in each annulus normalized such that, neglecting radial migration, a given gradient is reproduced (see Appendix A). Here we’ve adopted a double exponential with scale radii $r_t = 2.5$ kpc, $r_T = 2.0$ kpc, and $\Sigma_T/\Sigma_t = 0.27$ at $R_{\text{gal}} = 0$ (Bland-Hawthorn & Gerhard 2016). Both are plotted as dotted black lines in Fig. 8, and the sum as a solid black line.

- Surface density gradient from model with inside-out SFH, diffusion migration, and $\tau_\star^{\text{mol}} = (2 \text{ Gyr})(t/t_0)^{1/2}$ plotted in Fig. 8 as well (stars in red and gas in blue). Radial migration indeed didn’t change the overall scaling of Σ_\star with R_{gal} at the radii that we care about in this paper ($\gtrsim 3$ kpc), only introducing scatter. Gas disk appears to be well-fit by a single-exponential with scale radius of $\sim 3\text{-}4$ kpc.

- Increase in Σ_\star at $R_{\text{gal}} \lesssim 2$ kpc likely due to stellar populations finding bulge or pseudobulge star particles as analogs and migrating inward. Comment further on this, and plot PDFs of the kinematically decomposed star particles from h277: essentially zero bulge and pseudobulge star particles with either birth or final radii $\gtrsim 3$ kpc.

3.2 Metallicity

- Scaling of η with R_{gal} based on reproducing the observed mode($[\alpha/\text{H}]$)- R_{gal} trend, neglecting radial migration (see § 2.5). The target gradient is shown in a solid black line in Fig. 9.

- Gradient is indeed recovered in $[\text{O}/\text{H}]$, and radial migration appears to only induce scatter. While Fe did not enter into our

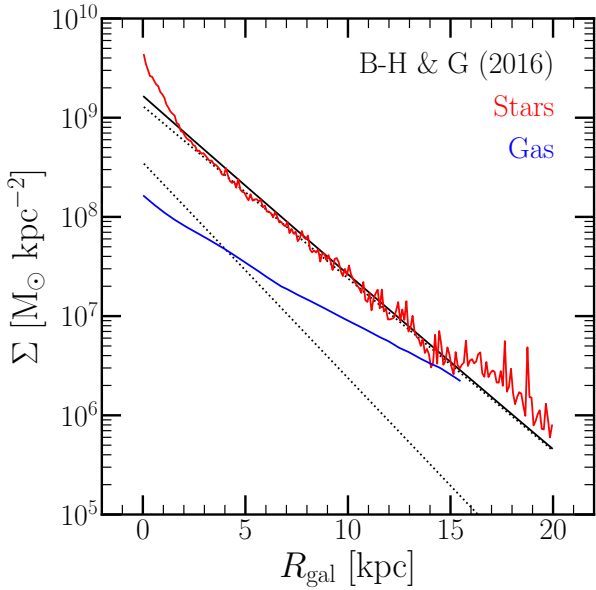


Figure 8. The surface density of gas (blue) and stars (red) as predicted by our model with an inside-out SFH, diffusion migration, and $\tau_\star^{\text{mol}} = (2 \text{ Gyr})(t/t_0)^{1/2}$. The dotted black lines denote the exponential fit to the thin- and thick-disk profiles reported by Bland-Hawthorn & Gerhard (2016), with the black solid line denoting the sum of the two, all renormalized to imply the same total stellar mass within the disk.

procedure for setting the metallicity gradient, the model predicts a similar gradient for [Fe/H].

- Metal-poor and α -enhanced tail in the inner galaxy predicted by all models.
- Details of the [O/Fe] gradient seem to be sensitive to differences in our SFHs.
- Constant SFH is the only model in which the present-day gas phase gradient matches the stellar gradient at all radii. In remaining models, the present-day gas-phase abundance is above the majority of the stars because the star formation rate has decreased.
- Stellar gradient is somewhat shallower in the late-burst model; this is because of the dilution associated with the starburst. Target gradient represents the equilibrium abundance at all radii, and we deliberately perturbed it from equilibrium, so any deviations from the expectation are a consequence of that.
- Late-burst model has super-equilibrium gas phase abundance at the present day. Can be seen in the break in the gas phase gradient in the outer-burst as well. This is a consequence of the starburst - in infall driven starbursts, re-enrichment can produce super-equilibrium abundances which then decay back to the equilibrium abundance as the star formation rate declines (Johnson & Weinberg 2020).

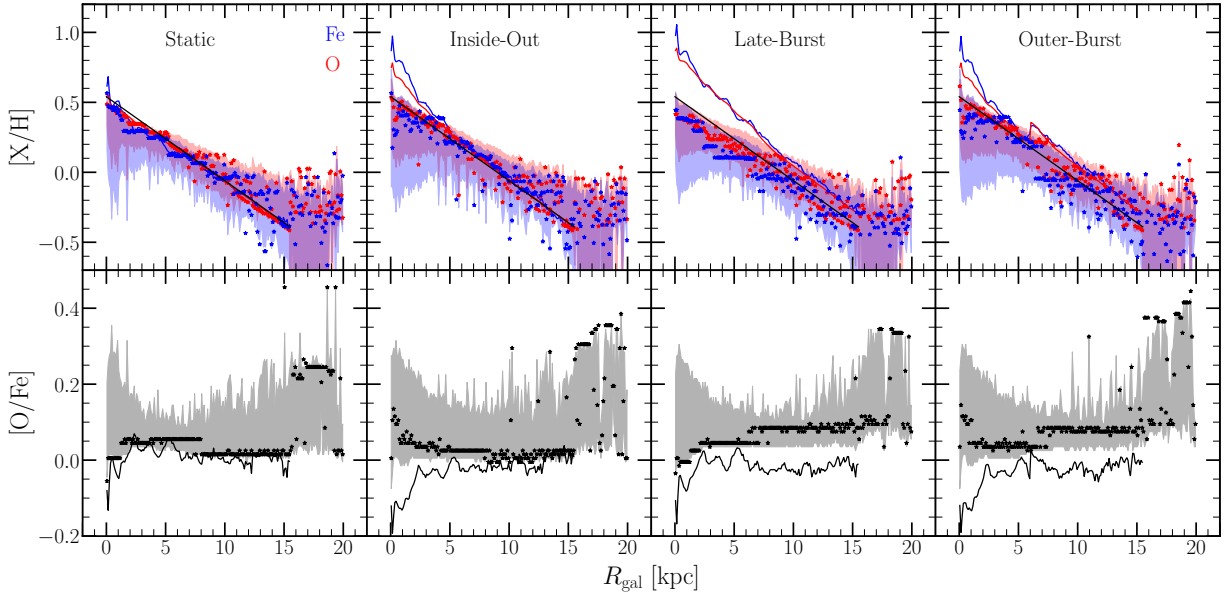


Figure 9. Radial abundance gradients in [O/H] (top, red) [Fe/H] (top, blue), and [O/Fe] (bottom) for our four fiducial SFHs - constant (far left), inside-out (left-middle), late-burst (right-middle), and outer-burst (far right). We plot the gas phase abundance at the present day as a function of Galactocentric radius in solid lines. Stars denote the mode of the stellar MDF of the 100-pc width annulus at a given radius, with shaded regions marking the 16th and 84th percentiles thereof. Black lines in the top panels denote our target $[\alpha/\text{H}]$ gradient of mode($[\alpha/\text{H}]$) = +0.3 at $R_{\text{gal}} = 4$ kpc with a slope of -0.06 kpc $^{-1}$.

4 METALLICITY SPACE

- Predicted [O/Fe]-[Fe/H] tracks for the diffusion model show significant deviations from the post-processing model, and these variations are due to the SN Ia rate varying in response to radial migration. This challenges the assumption that stars don't contribute to nucleosynthetic yields beyond their birth radius; that is, if a statistically significant fraction of stars are expected to migrate significantly from their birth radius when they're young ($\lesssim 2$ Gyr), this approximation is invalid. This is proof of concept that the radial migration of yields can occur as a consequence of the radial migration of stars.

- For each zone, VICE provides in its outputs the rates of infall and star formation, the mass of the ISM, and the relevant abundance information for each element along with the associated MDFs at the final timestep. To determine the SN Ia rates, we therefore have to approximate from the output.

- The time-derivative of the mass of Fe in a given annulus is given by:

$$\dot{M}_{\text{Fe}} \approx y_{\text{Fe}}^{\text{CC}} \dot{M}_{\star} + y_{\text{Fe}}^{\text{Ia}} \langle \dot{M}_{\star} \rangle_{\text{Ia}} - \frac{M_{\text{Fe}}}{M_g} \dot{M}_{\star} (1 + \eta(R_{\text{gal}}) - r) \quad (16)$$

where this is an approximation because in detail, there is a small contribution from AGB stars, and the recycling in the simulation is done continuously, whereas here we simply take $r \approx 0.4$ (appropriate for a Kroupa IMF; Weinberg et al. 2017). This equation can be derived from the Weinberg et al. (2017) analytic models assuming CCSN and SN Ia enrichment for Fe with instantaneous recycling of previously produced Fe. VICE's science documentation could also be referenced here; it has a nice detailed section on its treatment of each term in handling enrichment rates³. Re-

arranging this for the term describing the rate of injection due to SNe Ia events, and normalizing by M_{Fe} yields the following proxy with units of frequency:

$$\frac{y_{\text{Fe}}^{\text{Ia}} \langle \dot{M}_{\star} \rangle_{\text{Ia}}}{M_{\text{Fe}}} \approx \frac{\dot{M}_{\text{Fe}}}{M_{\text{Fe}}} - y_{\text{Fe}}^{\text{CC}} \frac{\dot{M}_{\star}}{M_{\text{Fe}}} + \frac{\dot{M}_{\star}}{M_g} (1 + \eta(R_{\text{gal}}) - r) \quad (17)$$

This term on the left-hand side can be substituted with $m_{\text{Fe}}^{\text{Ia}} \dot{N}_{\text{Ia}} / M_{\text{Fe}}$, where $m_{\text{Fe}}^{\text{Ia}}$ is the average mass of Fe produced by a single SN Ia event, and \dot{N}_{Ia} is the SN Ia rate itself. For this reason, this equation constitutes a straight-forward proxy for the SN Ia rate at any given time. This is the proxy that's plotted in the right-hand panel of Fig. 10, with multiplicative factors added for visual clarity.

- Some folks have assumed tracks in the [O/Fe]-[Fe/H] plane to infer birth radii for observed stars. We caution against inferring birth radii in this way for high- α stars, because radial migration may cause one to infer a considerably wrong birth radius, provided they're assuming a post-processing migration model. This however doesn't seem to affect the low- α sequence. It's possible that an additional dimension such as age could mitigate these issues.

- Variability in the SN Ia rate shows high-amplitude on Gyr timescale, low-amplitude white-noise on shorter timescales. In general the time-averaged rates follow the expectation from the post-processing model. Fractional amplitude of variability increases with Galactocentric radius.

- Demonstrate in the next section that this is a means with which to form α -rich and α -poor stars - or rather Fe-poor and Fe-rich, respectively.

- Fig. 11 shows a scatter plot of 10,000 randomly sample stellar populations in five bins of R_{gal} and three bins of $|z|$ ($R_{\text{gal}} = 3 - 5$ kpc, $5 - 7$ kpc, $7 - 9$ kpc, $9 - 11$ kpc, and $11 - 13$ kpc; $|z| = 0 - 0.5$ kpc, $0.5 - 1$ kpc, and $1 - 2$ kpc). These are the same bins and same scheme for organizing the panels as in Fig. 4 of Hayden et al. (2015).

³ https://vice-astro.readthedocs.io/en/latest/science_documentation/enrichment/index.html

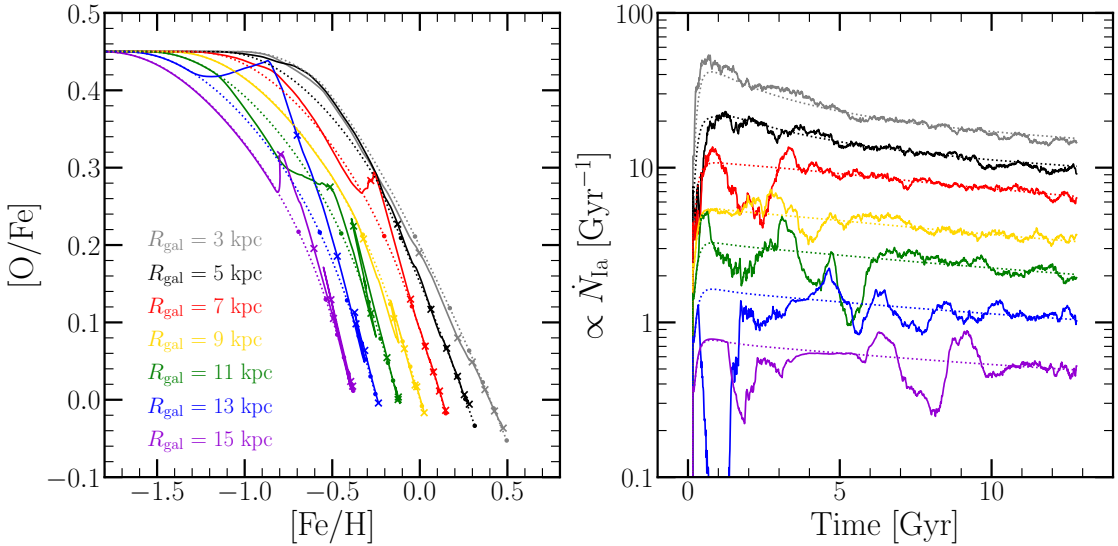


Figure 10. **Left:** Evolutionary tracks for the gas phase in the [O/Fe]-[Fe/H] plane for models with $\tau_{\star}^{\text{mol}} = (2 \text{ Gyr})(t/t_0)^{1/2}$, our inside-out SFH, and either post-processing (dotted lines) or diffusion (solid lines) migration models. We plot tracks for seven annuli, color-coded according to their Galactocentric radius and denoted by the legend in the lower-left. We mark simulation times of 2, 4, 6, 8, 10, and 12.7 Gyr in X's for the diffusion model and points for the post-processing model. **Right:** The proxy for the SN Ia rate defined in equation (17) as a function of simulation time for the same annuli as in the left-hand panel. We multiply rates at each radii here by various prefactors in the interest of clarity.

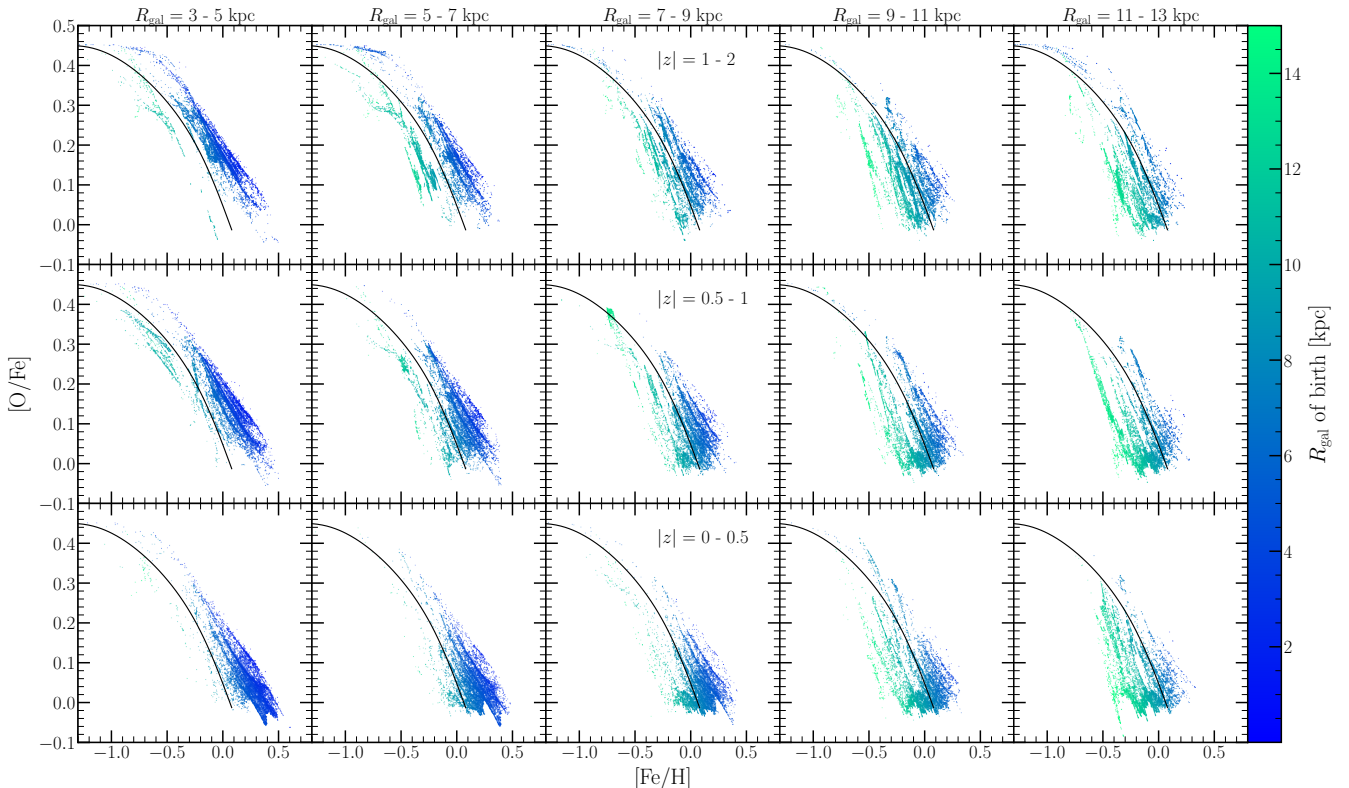


Figure 11. [O/Fe]-[Fe/H] diagrams for 15 galactic regions spanning five bins in R_{gal} and $|z|$. Each region has its own panel, with radial bins shown in columns denoted at the top of the figure, and with $|z|$ bins shown in rows denoted in text in the middle column panels. In each panel, we plot $N = 10,000$ points sampled from our simulated stellar populations in each region predicted by our inside-out SFH, where the probability of sampling is proportional to the present-day mass of each stellar population. In all panels points are color-coded according to the Galactocentric radius of birth of the stellar population. For reference, we plot in a solid black line in all panels the gas-phase [O/Fe]-[Fe/H] track predicted by the same SFH in the $R_{\text{gal}} = 8 \text{ kpc}$ annulus, but with the post-processing migration model; this curve is the same in all panels.

- The width of the low- α sequence predicted by the model comes from radial migration, in agreement with the prediction of Schönrich & Binney (2009).
- The low- α sequence shifts from a high [Fe/H] locus at small R_{gal} to low [Fe/H] at high R_{gal} , in agreement with the observed distributions in APOGEE presented in Hayden et al. (2015).
- High- α stars are most prevalent at low R_{gal} and high $|z|$, and conversely for the low- α stars, also in agreement with Hayden et al. (2015).

– Similar results are found for different SFHs. This suggests that this observed result is a natural consequence of stellar migration.

– Only minor difference worth noting is that the starburst models predict a slightly higher characteristic [O/Fe] ($\sim +0.1$) for the low- α sequence. This is a natural consequence of the starburst.

5 THE AGE-[α /FE] RELATION

- Feuillet et al. (2019) make use of APOGEE DR14 stars where there are Gaia parallax measurements available (Gaia Collaboration et al. 2018). With their spatial cuts, the final sample consisted of 77,562 stars. In bins of [O/Fe], they assume a gaussian age distribution, and fit the mean and standard deviation to the observed sample. Because they assume a gaussian, they would report an equal mean and median.
- The stellar populations from our simulations have different masses, so the age-distributions must be weighted by mass, since that scales with the number of stars that each stellar population represents.
- Our age distributions in the vast majority of [O/Fe] bins are highly non-gaussian, so we compare to Feuillet et al. (2019) based on the predicted mass-weighted median age in [O/Fe] bins (i.e. the age which 50% of the stellar mass in a given bin is younger than). For these reasons the comparison between our simulations and Feuillet et al. (2019) isn't exactly one-to-one.

5.1 The Impact of Radial Migration

- Fig. 12 shows a comparison between the predicted age-[α /Fe] relations in the solar annulus for our four migration models assuming our inside-out SFH.
- All models show reasonable agreement with the Feuillet et al. (2019) data; the population-averaged trend appears insensitive to the assumed migration model.
- Diffusion predicts the most intrinsic scatter, followed by linear, then sudden, then post-processing. Further demonstration that under certain migration models, the radial migration of nucleosynthetic yields is statistically significant.
- This mechanism can produce populations of Fe-poor or Fe-rich stars, which can be misinterpreted as α -rich or α -poor stars. Due to young stars migrating into or out of a given annulus, the SN Ia rate may be higher or lower than the expectation from a post-processing migration model. If this difference in the SN Ia rate is sustained for of order one depletion time, the ISM will be either Fe-poor or Fe-rich, and the stars that form there will inherit that composition.⁴ The stars that form out of that patch of ISM can then migrate to the solar

⁴ Potentially note the Weinberg et al. (2017) definition: $\tau_{\text{dep}} \equiv \tau_{\star}/(1+\eta - r)$. Even with τ_{\star} as high as ~ 5 Gyr at large Galactocentric radii, depletion times are still short due to the high values of η there.

annulus. This effect is most significant at large Galactocentric radii where the fractional amplitude of the variability in the SN Ia rate is largest, and for that reason the young Fe-poor population predicted by our diffusion model originates at large radii ($\gtrsim 12$ kpc).

• Silva Aguirre et al. (2018) demonstrated that the observed young α -rich stars in the solar annulus have kinematics similar to the rest of the high- α population, and suggested that this may be the result of stellar mergers or mass transfer events, producing a population of truly old stars masquerading as young stars. This would imply that the observed young α -rich population is actually just older, high- α stars that have gone through some special class of stellar evolution. Our model predicts intrinsically young, Fe-poor stars to explain the observations, but these interpretations are not mutually exclusive. Ascertaining the origins of this population therefore has implications for which of the migration models investigated here is the most realistic.

5.2 The Impact of the Star Formation SFH

- Fig. 13 shows a comparison between the predicted age-[α /Fe] relations in the solar annulus for our four SFHs assuming diffusion migration.
- Constant and inside-out SFHs describe the observed data the best. Both late starburst models show a population-averaged increase in [α /Fe] at young ages which is not observed in the data. This challenges the results of Isern (2019) and Mor et al. (2019), suggesting that these results on the Milky Way recent SFH are not consistent with chemical evolution models.
- Below [O/Fe] $\approx +0.1$, the Feuillet et al. (2019) data seem to follow a slightly steeper age-[α /Fe] than our inside-out model predicts. This likely points to inaccuracies in the detailed form of the SFH or the SN Ia DTD, both of which are within the uncertainties of these models.

5.3 Beyond the Solar Annulus

- Fig. 14 presents a comparison of our simulation data to the Feuillet et al. (2019) observational data in 12 Galactic regions assuming the inside-out SFH.
- In the disk, the inside-out SFH is a reasonable description of the data for ages $\lesssim 5$ Gyr, above which the median ages are overpredicted relative to Feuillet et al. (2019). Far from the midplane, our model overpredicts the ages at nearly all abundances where Feuillet et al. (2019) have data, with the exception of the $R_{\text{gal}} = 7 - 9$ kpc and $|z| = 0.5 - 1$ kpc region.
- Differences in ages are interesting though - nearly everywhere we overpredict ages relative to Feuillet et al. (2019), their data are reasonably described by the stellar populations from our simulations that we would classify as Fe-poor. Especially noticeable in the $R_{\text{gal}} = 5 - 7$ kpc, $|z| \leq 0.5$ regions (i.e. lower-left panel), where the observed data also show an abrupt increase in age near the maximum [O/Fe] ratio of one particular Fe-poor population, with one data point that agrees with the population-averaged trend from the simulation.

– Taking the Feuillet et al. (2019) data at face value, this would suggest that our simulation is overpredicting the rate of Fe injection from SN Ia, implying a SN Ia DTD whose characteristic timescales are longer than we employ here, thus slowing the decrease of [α /Fe] with time.

– Feuillet et al. (2019) made use of APOGEE DR14 data for which Gaia parallax measurements are available. With their quality cuts the final sample consisted of 77,562 stars. Taking

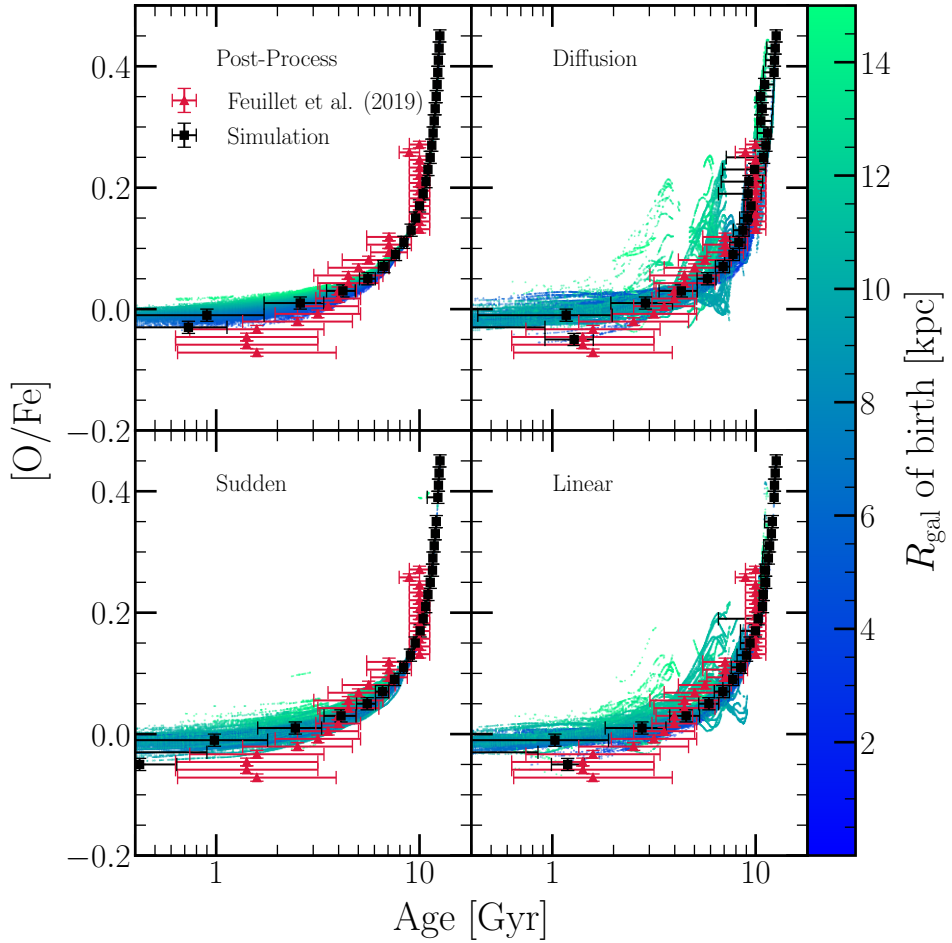


Figure 12. A comparison of the predicted age-[O/Fe] relation for the solar annulus ($R_{\text{gal}} = 7 - 9$ kpc and $|z| \leq 0.5$ kpc) between the post-processing (upper left), diffusion (upper right), sudden (lower left), and linear (lower right) migration models, assuming our inside-out SFH and $\tau_{\star}^{\text{mol}} = (2 \text{ Gyr})(t/t_0)^{1/2}$. Red triangles and error bars denote the observed mean age and dispersion thereof in bins of [O/Fe] as reported by Feuillet et al. (2019); here we include only the bins containing at least 15 stars. Black squares denote the mass-weighted median age in 0.02-dex bins in [O/Fe], with error bars denoting the 16th and 84th percentiles of the mass-weighted age distribution in those bins. Points in the background denote each individual stellar population from the simulation with a final position in the solar annulus, color-coded according to their Galactocentric radius of birth.

the simulation results at face value, this would suggest that APOGEE+Gaia target selection favors the stars we would classify as Fe-poor.

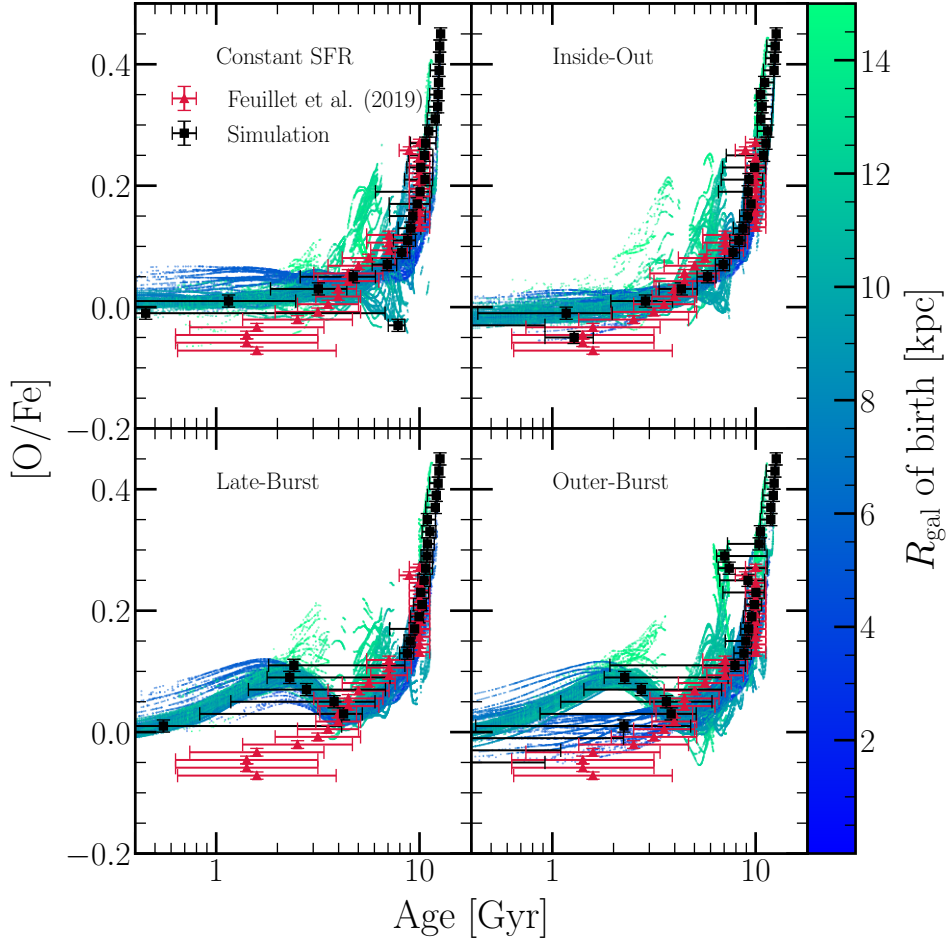


Figure 13. The same as Fig. 12, instead comparing the impact of our constant (upper left), inside-out (upper right), late-burst (lower left), and outer-burst (lower right) SFHs, assuming diffusion migration and $\tau_{\star}^{\text{mol}} = (2 \text{ Gyr})(t/t_0)^{1/2}$.

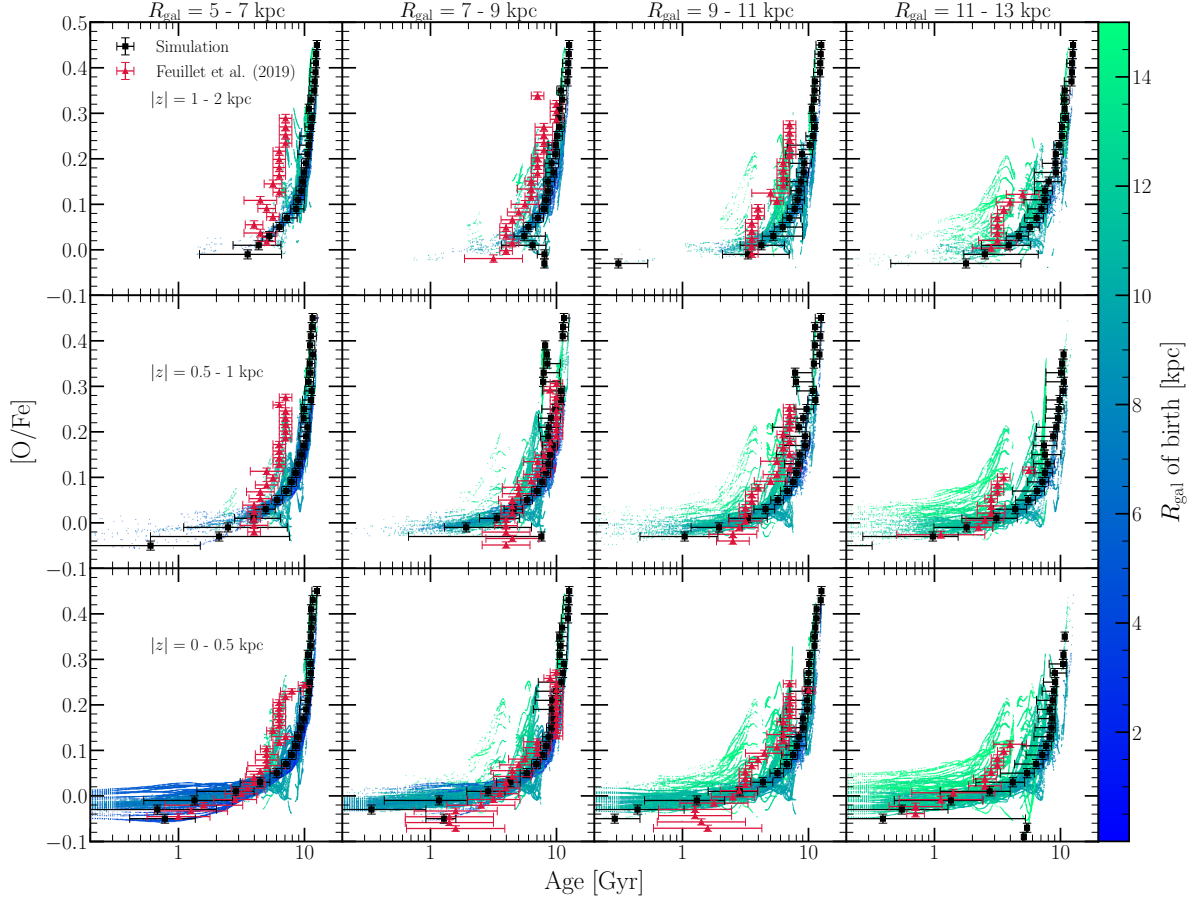


Figure 14. The age-[O/Fe] relation in difference galactic regions predicted by our inside-out SFH with $\tau_*^{\text{mol}} = (2 \text{ Gyr})(t/t_0)^{1/2}$ and diffusion migration. Bins in Galactocentric radius are shown in columns, and labeled at the top. Bins in the height $|z|$ above/below the disk midplane are shown in rows, noted in the left-hand column. Red triangles and error bars denote the observed mean age and dispersion thereof in bins of [O/Fe] as reported by Feuillet et al. (2019); here we include only the mass bins containing at least 15 stars. Black squares denote the mass-weighted median age in 0.02-dex bins in [O/Fe], with error bars denoting the 16th and 84th percentiles of the mass-weighted age distribution in those bins. Points in the background denote each individual stellar population from the simulation with a final position in that Galactic region, color-coded according to their Galactocentric radius of birth.

6 THE AGE-METALLICITY RELATION

- Fig. 15 shows a comparison of the predicted age-[O/H] for $|z| \leq 0.5$ stars in four bins in Galactocentric radius between our four fiducial SFHs and the Feuillet et al. (2019) data. Fig. 16 shows the same comparison but for the age-[Fe/H] relation.

• For a constant SFR, our model predicts a non-monotonic AMR at all radii for both O and Fe; that is, the most metal-rich stars in a given annulus are not the youngest stars. Under this model, the metallicity of the youngest stars reflects the equilibrium abundance at a given radius. This is an indication that the turnover in the observed AMR is tied to the abundance gradient in our models. This supports the notion first raised in Feuillet et al. (2018) using the Weinberg et al. (2017) analytic models that the non-monotonicity of the observed AMR is a consequence of radial migration. At any given annulus, a metallicity significantly different than the equilibrium abundance is an indication that that star migrated a significant distance, and is thus necessarily old because it would need an adequate amount of time to do so. This effect is also strong enough that in the 11 - 13 kpc bin, the model predicted AMR is nearly monotonically increasing due to this annulus's position at the tail of the abundance gradient.

- Inside-out SFH tends to suppress the formation of this so-called young metal-rich population in the inner galaxy. The highest metallicity stars are not predicted to be significantly older than lower

metallicity stars at 5 - 7 kpc in both [O/H] and [Fe/H], and also at 7 - 9 kpc in [Fe/H]. In other words, the inside-out model predicts an AMR for the inner Milky Way that follows a different trend than suggested by Feuillet et al. (2019). In the 9 - 11 and 11 - 13 kpc bins, the inside-out model in general overpredicts ages of solar and supersolar metallicity stars, though the agreement is reasonable at subsolar metallicity.

• In the late-burst model, the agreement between the simulation prediction and the observational results at 5 - 7 kpc shows a noticeable improvement from the inside-out model. This is because the late-burst model forms an excess of mildly subsolar ($-0.5 \lesssim [\text{O/H}]$, $[\text{Fe/H}] \lesssim 0$) at ages of ~ 2 Gyr. This decreases the median age at that metallicity, where the inside-out model has its biggest discrepancy with the observations at that radius. In the solar annulus, there is little difference in the predicted age-[O/H] relations between inside-out and late-burst, but there is an improvement for Fe for the same reason as before. Agreement is also improved for both elements in the 9 - 11 and 11 - 13 kpc bins; the trends are better reproduced in the burst model, though the ages of the most metal-rich stars are still overpredicted. Appears to be a slight offset between the predicted and observed AMR for Fe; this could point to any number of minor modifications.

– Highest metallicity bins at 5 - 7 kpc are the effect of poor statistics. We're taking the median of a distribution that is bimodal, so the median age there is extremely sensitive to the detailed timing of the starburst.

– Improvement in agreement due not only to the late starburst but also to the effect of dilution - for this reason, not many young, super-solar metallicity stars form simply because of a global decrease in metallicity in the model Milky Way's evolution, visible in the colored points on each panel.

• Outer-burst predicted AMR is particularly sensitive to our decision to neglect radial gas flows, particularly at 5 - 7 kpc because the burst is assumed to occur at ≥ 6 kpc in this model, so we caution that it's easy to over-interpret the quantitative interpretations of this model. In detail, a more realistic model involving radial gas flows would show some metal-poor gas moving inward and carry the effect of dilution in some capacity down to $R_{\text{gal}} = 0$. No major differences in the population-averaged predictions between late- and outer-burst models aside from the highest metallicity bins in the inner galaxy where the age distribution was bimodal in the late-burst model.

• Potentially worth noting that the solar annulus is reasonably described by all four models for both O and Fe. On these grounds we'd advise future studies doing a detailed comparison of observed and model-predicted AMRs to consider multiple Galactic regions.

• Conclude that the AMR reported by Feuillet et al. (2019) is better described by our late starburst models than the inside-out model, while the age-[α/Fe] relation also reported by Feuillet et al. (2019) is better described by the inside-out model. What can reconcile the differences between the two.

– Likely not an indication that we need to relax our assumptions about the detailed timing of the starburst at a given radius (i.e. our assumptions about $f(t|R_{\text{gal}})$ in the burst models). Any significant global starburst will produce a global α -enhancement that isn't seen in the observed data (see the comparison of our models to the Feuillet et al. (2019) data in § 5).

– Possibly there was a dilution event with no significant resulting starburst (this could happen if the majority of the accreted gas was HI that has not yet cooled). With ongoing star formation but

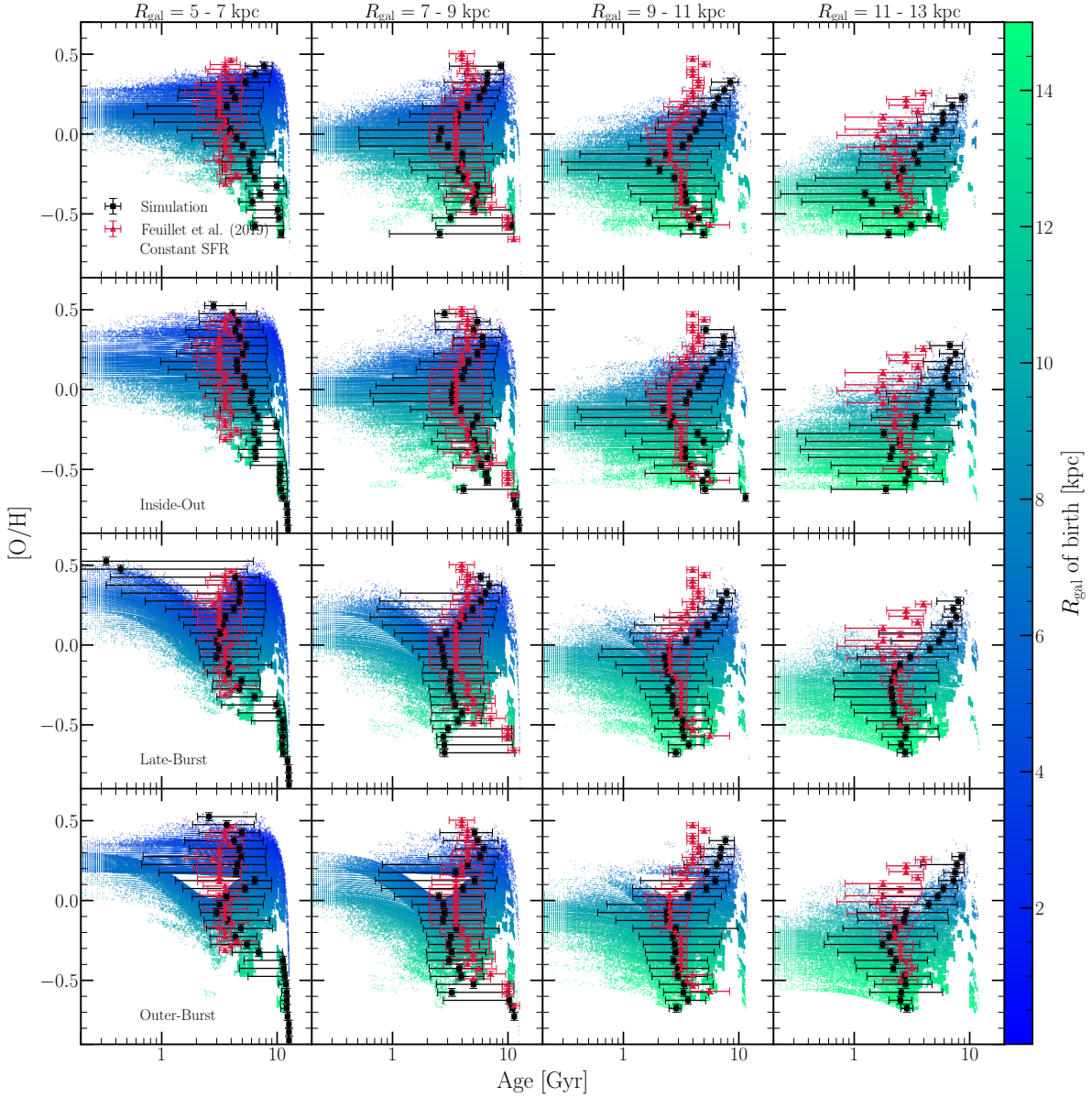


Figure 15. The age- $[\alpha/\text{H}]$ relation predicted by our constant (top), inside-out (top middle), late-burst (bottom middle), and outer-burst (bottom) SFHs for $R_{\text{gal}} = 5 - 7 \text{ kpc}$ (left), $7 - 9 \text{ kpc}$ (left middle), $9 - 11 \text{ kpc}$ (right middle), and $11 - 13 \text{ kpc}$ (right). Each panel plots only the $|z| \leq 0.5 \text{ kpc}$ population. Background points, red triangles with error bars, and black squares with error bars are as in Fig. 14, but with our binned, simulation quantified in 0.05-dex bins in $[\text{O}/\text{H}]$.

not a starburst, re-enrichment and the ensuing α -enhancement would be significantly slower, potentially to the point that no significant α -enhancement is predicted. With dilution playing a role in the AMR predicted by the burst models, it's possible that its agreement with the data could be retained.

6.1 Beyond the Midplane

- Fig. 17 shows the predicted age- $[\text{O}/\text{H}]$ relation in 12 Galactic regions from the late-burst SFH in comparison to the Feuillet et al. (2019) data. Fig. 18 shows the same thing, but for the age- $[\text{Fe}/\text{H}]$ relation.
- With increasing $|z|$, the age distribution of stellar populations

moves quickly to high ages, in qualitative agreement with observations.

- Off the midplane, ages are in general overestimated at nearly all radii in both O and Fe, particularly for the $|z| = 1 - 2 \text{ kpc}$ regions.
- Find similar results for our other models. What could be causing this discrepancy with the observations?

– We assumed that the disk is vertically and azimuthally well-mixed. Could this point to a breakdown in the assumption of efficient vertical mixing?

– The dynamical history of our model is not the Milky Way's dynamical history; it's h277's dynamical history. Perhaps the Milky Way had a dynamical disturbance to the disk that kicked a bunch of younger stars to high $|z|_{\text{max}}$ orbits (e.g. potentially the Sagittarius Stream).

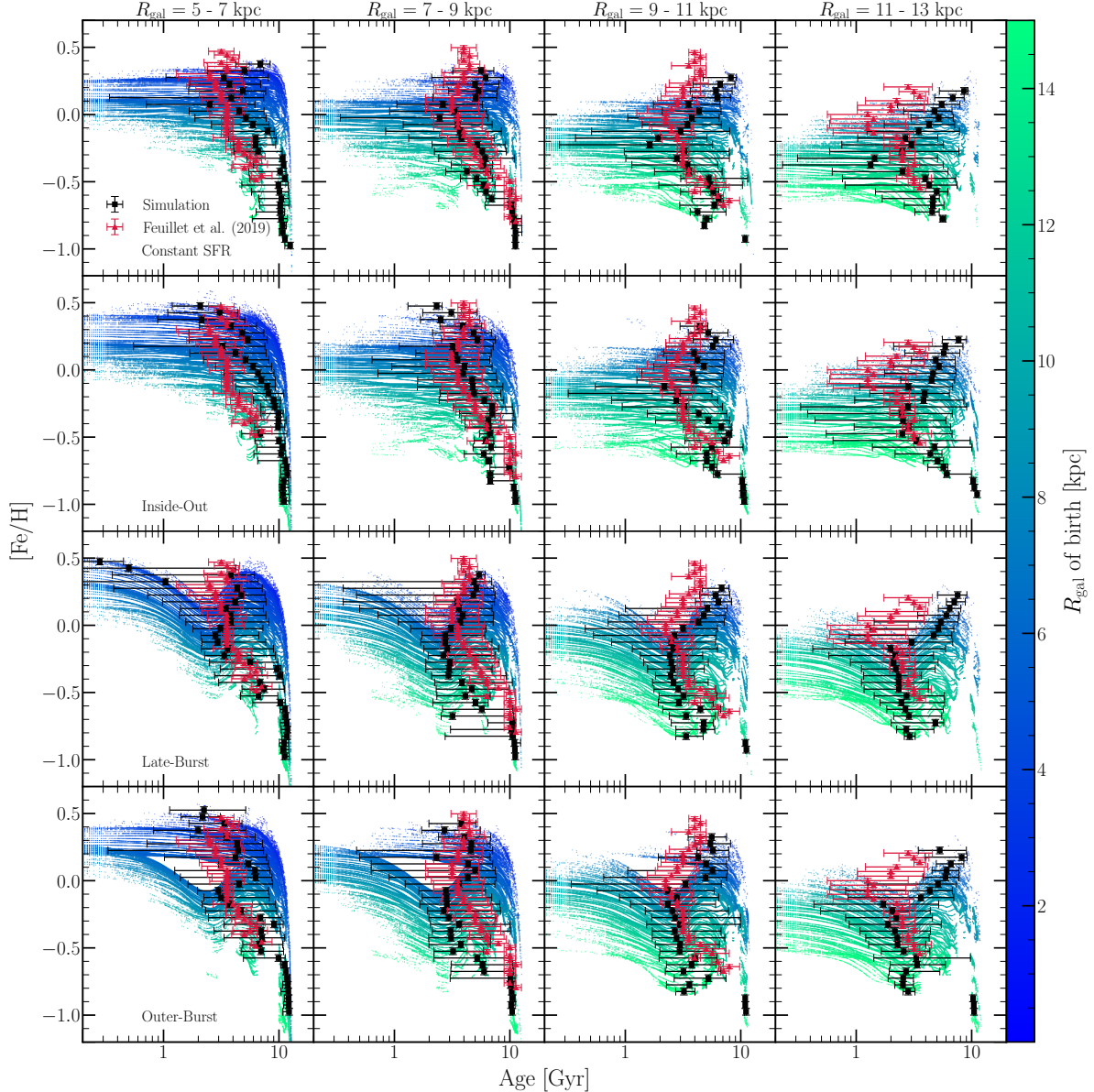


Figure 16. The same as Fig. 15, but for the age-[Fe/H] relation.

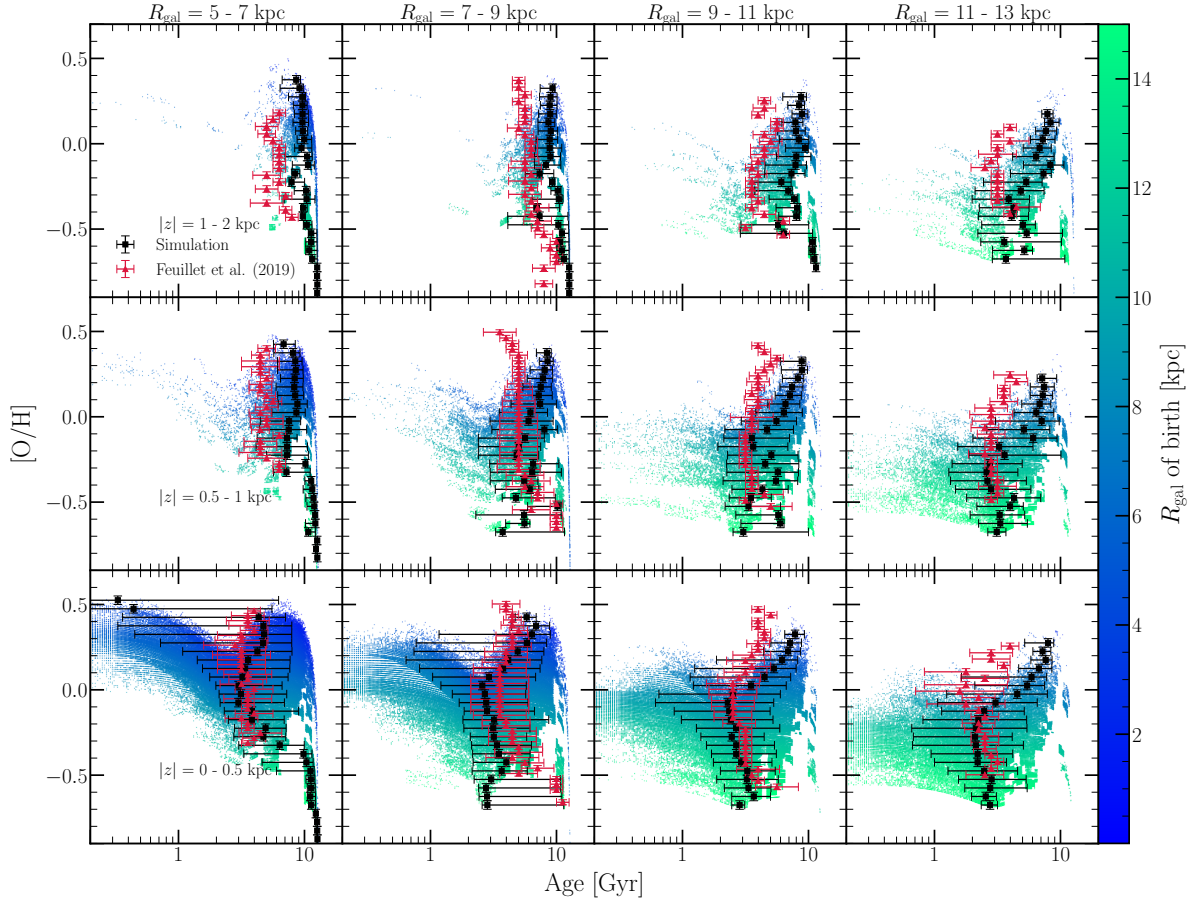


Figure 17. The same as Fig. 14, but for the age-[O/H] relation, the late-burst rather than the inside-out SFH, and with our binned, simulated relation quantified in 0.05-dex bins in [O/H].

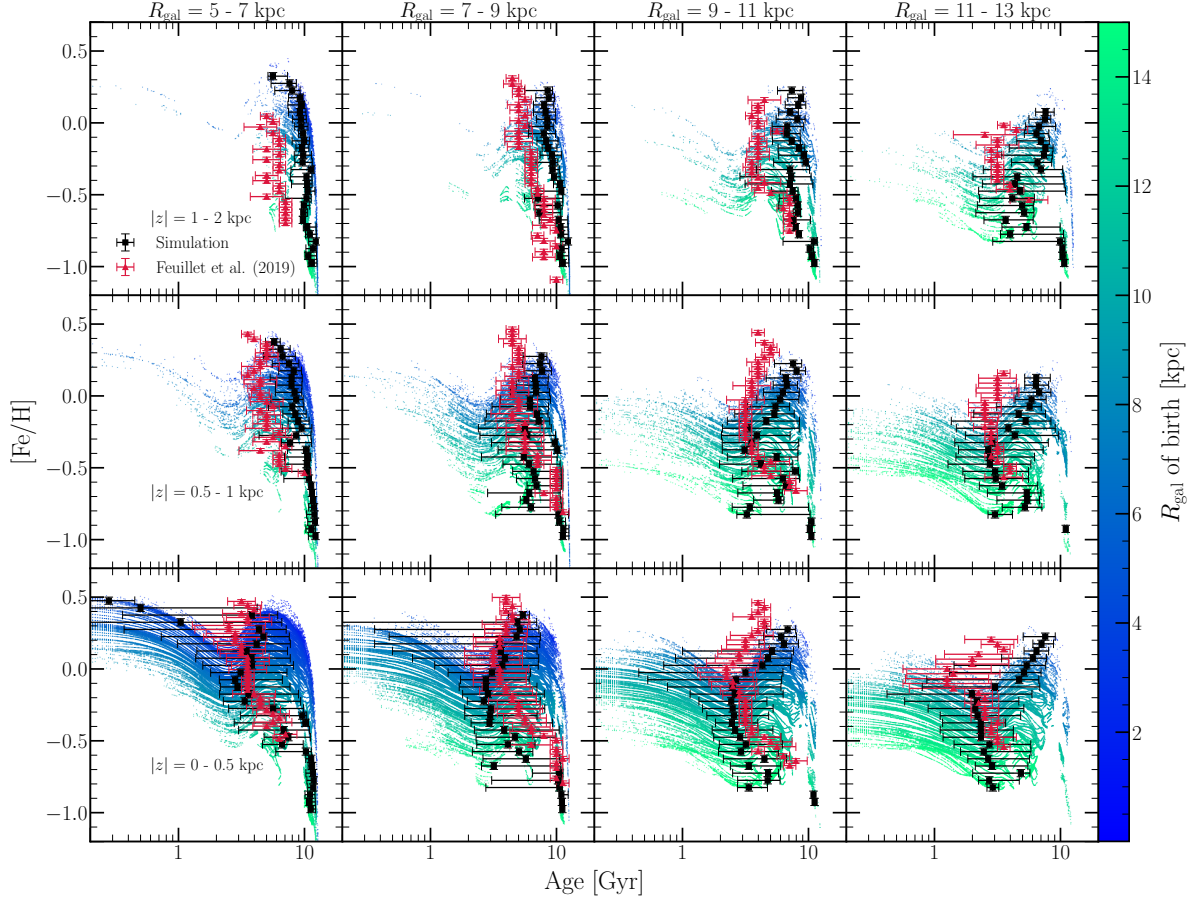
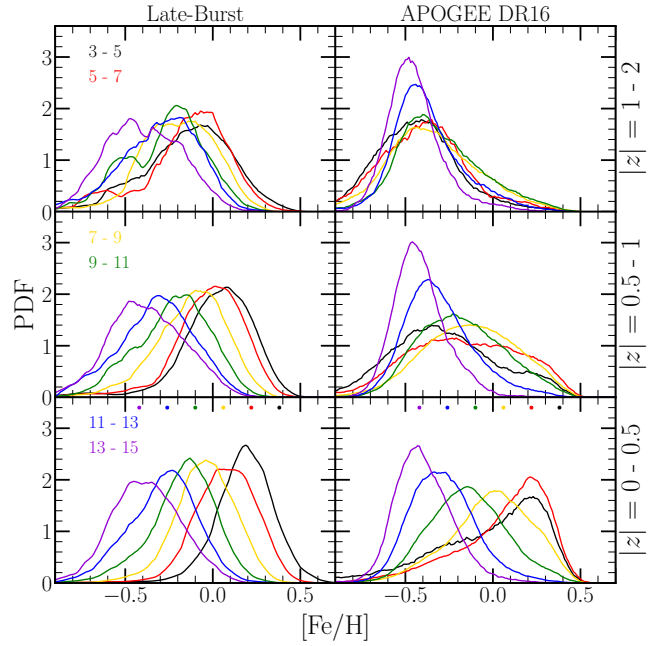


Figure 18. The same as Fig. 14, but for the age-[Fe/H] relation, the late-burst rather than the inside-out SFH, and with our binned, simulated relation quantified in 0.05-dex bins in [Fe/H].

7 METALLICITY DISTRIBUTION FUNCTIONS



7.1 [O/H] and [Fe/H]

- MDFs in bins of Galactocentric radius are a fundamental observable to test the validity of any chemical evolution model.
- Previously known that the MDFs in the disk midplane as observed in APOGEE show mode $[\alpha/\text{H}]$ and $[\text{Fe}/\text{H}]$ abundances that depend on Galactocentric radius, with a skew-negative distribution in the inner Galaxy and a skew-positive distribution in the outer Galaxy. Off the midplane, the MDFs merge and converge on $[\alpha/\text{H}] \approx [\text{Fe}/\text{H}] \approx -0.5$ (Hayden et al. 2015; Weinberg et al. 2019). This result is replicated in the left-hand column of panels in Fig. 19 and Fig. 20.

Figure 19. Metallicity Distribution Functions in $[\text{Fe}/\text{H}]$ predicted by our late-burst model (left) and as observed in APOGEE DR16 (right), for stars and simulated stellar populations with present day $|z| = 0 - 0.5$ kpc (bottom), $0.5 - 1$ kpc (middle), and $1 - 2$ kpc (top). MDFs are shown in bins of Galactocentric radius: 3 - 5 kpc (black), 5 - 7 kpc (red), 7 - 9 kpc (yellow), 9 - 11 kpc (green), 11 - 13 kpc (blue), and 13 - 15 kpc (purple). The points near the top of the bottom panels denote what the mode abundance would be if it followed our target gradient of $[\text{Fe}/\text{H}] = +0.3$ at $R_{\text{gal}} = 4$ kpc and a slope of -0.08 kpc^{-1} , assuming the inner radius of each bin (i.e. there is no point plotted for 15 kpc). All distributions are smoothed with a box-car width of $[\text{Fe}/\text{H}] \pm 0.1$.

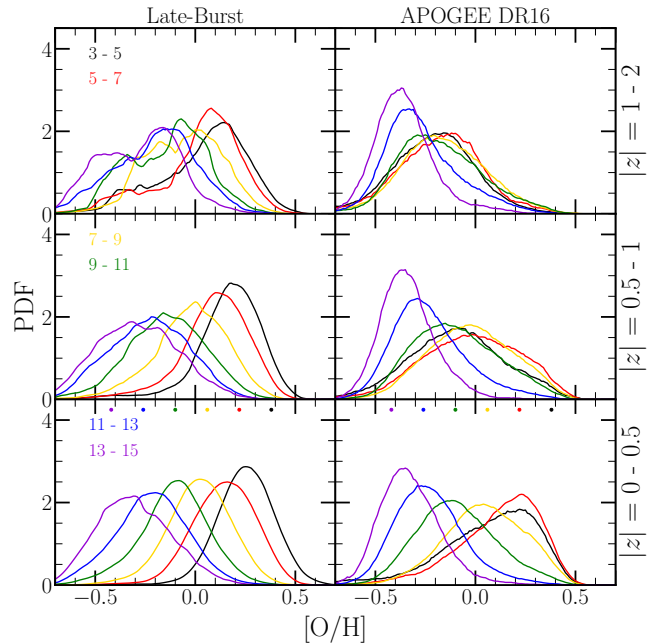


Figure 20. The same as Fig. 19, but for $[\text{O}/\text{H}]$.

– Similar mode $[\text{O}/\text{H}]$ and $[\text{Fe}/\text{H}]$ between the 3 - 5 and 5 - 7 kpc in the APOGEE observations. What could be the origin of

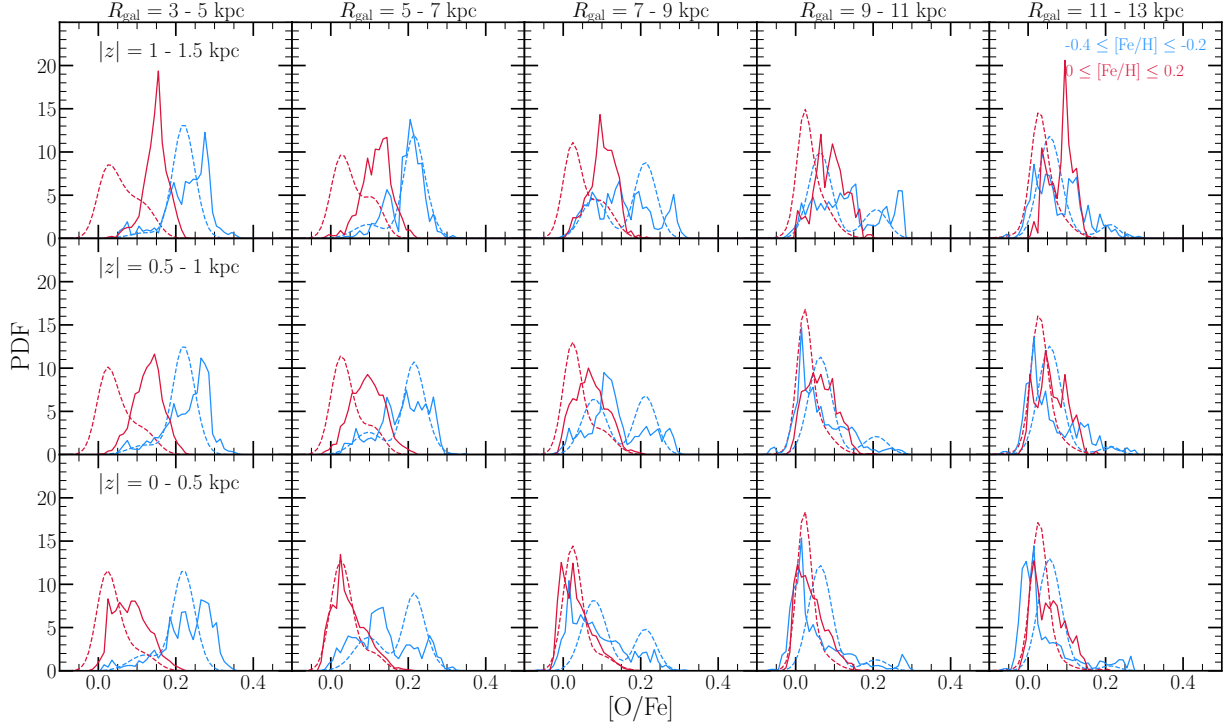


Figure 21. Predicted distributions in [O/Fe] in 15 Galactic regions and in two bins in [Fe/H]. Columns correspond to bins in R_{gal} , denoted at the top of each column. Rows correspond to bins in $|z|$, denoted in text in the left-hand column. Distributions are color-coded according to the [Fe/H] the sample is drawn from, denoted by the legend in the upper right panel. Solid lines denote that predicted by our inside-out SFH, while dashed lines denote the observed distributions from APOGEE DR16, quantified in Vincenzo et al. (2021, in prep.).

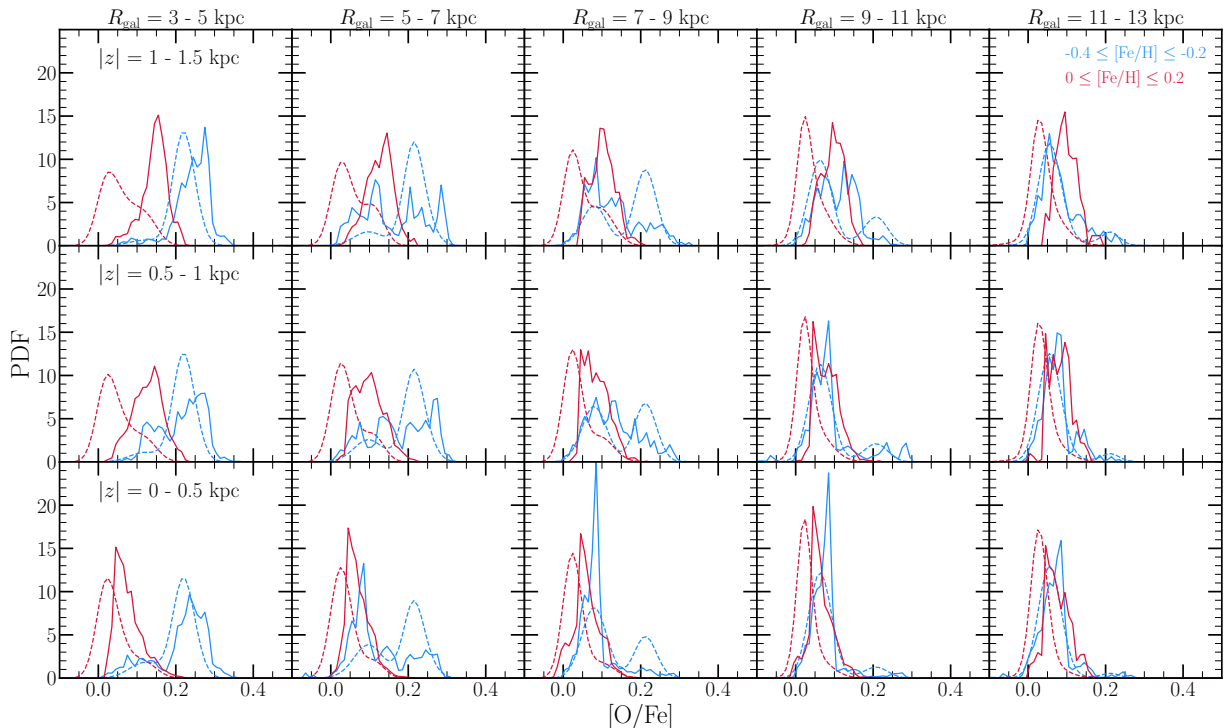


Figure 22. The same as Fig. 21, but with the solid lines denoting the predictions of our late-burst SFH.

this? Cessation of star formation in the inner Galaxy? (see Fig. 1 of [Peek 2009](#) and Fig. 2 of [Fraternali & Tomassetti 2012](#)). This would imply very few stars formed in the most metal-rich regions of the Galaxy, cutting off the MDF at high [O/H], [Fe/H].

- Left-hand panels of Figs. 19 and 20 show the distributions predicted by our late-burst model. They successfully replicate the qualitative result that the mode [X/H] varies with present-day Galactocentric radius, but fail to show a similar mode abundance between the 3 - 5 and 5 - 7 kpc bins. Potentially linked to the cessation of star formation in inner Galaxy ([Peek 2009](#); [Fraternali & Tomassetti 2012](#)).

• Beyond the midplane, our models fail to fully replicate the convergence of the MDFs at $[x/H] \approx -0.5$. The observed MDF at small radii shifts from skew-negative with a metal-rich mode to skew-positive with a metal-poor mode with increasing $|z|$. In our predicted MDFs for the inner galaxy, the mode does shift to lower [X/H], though not as low as in the observations. There is also very little change in skewness with $|z|$ predicted, in tension with observations.

– Could this point to a breakdown of our assumption that vertical mixing is efficient?

– Some discussion in § 6 that the Sagitarrius stream may be responsible for the young ages observed at high $|z|$ in [Feuillet et al. \(2019\)](#). This likely wouldn't solve the problem here, because our annuli are at or near equilibrium at the lookback times associated with the Sagitarrius dwarf's pericentric passages, meaning this effect would only kick high [X/H] stars to high $|z|$.

- We note that our models do a good job of producing a mode [X/H] abundance in each radial bin close to our target gradient. In the inner galaxy bins in Figs. 19 and 20, the predicted mode is moderately lower than the target, but this is due to the effect of dilution (see discussion in § 6). In our inside-out model, the difference in target and predicted mode [X/H] is considerably smaller.

7.2 [O/Fe]

- Fig. 21 show distributions in [O/Fe] in two bins of [Fe/H] across 15 Galactic regions predicted by our inside-out SFH (solid lines).

• Dashed lines denote the distributions quantified in Vincenzo et al. (2021, in prep). These are intended to simultaneously remove the effects of observational errors in [O/Fe] and the APOGEE selection function in these Galactic regions; that is, these are estimates of the *intrinsic* [O/Fe] distributions that, when convolved with observational uncertainties and the APOGEE selection function, would resemble the observed MDFs.

• We note that the inside-out model fails to reproduce a Milky Way-like bimodality. Such a model prediction would appear as good agreement between the solid and dashed lines in Fig. 21, but that is not the case. There may be decent agreement in a given metallicity bin and Galactic region, but the agreement would need to be seen everywhere and at all metallicities.

• In the inner galaxy, we overestimate the [O/Fe] of the highest [Fe/H] stars at all $|z|$, and the differences in the distributions gets smaller with increasing R_{gal} . The lower [Fe/H] bins don't seem to have this problem.

– Since these are in specific bins in [Fe/H], this is an indication that our model is overpredicting the O abundances of these stars, rather than underpredicting [Fe/H].

– This could point to various things. Perhaps the Milky Way has different gradients in [O/H] than [Fe/H], an effect which is not captured by these models. Perhaps the innermost radii of the Milky Way has some contamination from bulge stars, another effect which is not captured by our models.

- Fig. 22 shows the same thing as Fig. 21, but for the late-burst SFH.

• We note that this model does not predict a Milky Way-like bimodality either, and still suffers from the issues facing the inside-out model regarding the highest [Fe/H] stars in the inner Galaxy.

• While the notion that an $[\alpha/\text{Fe}]$ dichotomy can arise out of radial migration alone was put forth in [Schönrich & Binney \(2009\)](#), this suggests that an inside-out star formation history combined with stellar migration is not conducive to predicting this observed result. This is at odds with the findings of [Sharma et al. \(2020\)](#), who claim to reproduce the $[\alpha/\text{Fe}]$ dichotomy with an analytic chemical evolution model.

– **We'll need to be careful in our final draft of the paper so that our language here isn't too strong. Below I've given my honest critiques of the [Sharma et al. \(2020\)](#) paper.**

– They have a single SFH.

– They assume a functional form for [Fe/H] and $[\alpha/\text{Fe}]$ with time and radius, indicating that their $[\alpha/\text{Fe}]\text{-}[Fe/H]$ tracks are *not* model predictions, and are instead assumptions characterized *a priori* by radius and time. Rather than learning about the physical origins of the $[\alpha/\text{Fe}]$ dichotomy, we instead get a robust mathematical caricature of the data.

– They find a dichotomy in the $[\alpha/\text{Fe}]\text{-}[Fe/H]$ plane to arise out of a fast transition in the gas phase between high- α and low- α . In practice, we find that this is only the case if τ_{\star} is sufficiently short; analytic justification for this is also presented in [Weinberg et al. \(2019\)](#) (**We could potentially demonstrate this in Appendix B as well**). In this paper, we adopted the [Tacconi et al. \(2018\)](#) scaling of $\tau_{\star}^{\text{mol}}$ with redshift. We find that none of our models predict a τ_{\star} adequately short such as to produce an adequately fast transition between high- α and low- α sequences, as assumed in the [Sharma et al. \(2020\)](#) analysis.

– For these reasons, we believe our investigation to be more robust, physically motivated, and internally consistent than the [Sharma et al. \(2020\)](#) analysis.

• These findings suggest that an inside-out SFH combined with radial migration, even when a late starburst is taken into account (as motivated by the findings of [Isern 2019](#) and [Mor et al. 2019](#)), is *not* conducive to producing the observed $[\alpha/\text{Fe}]$ dichotomy. This suggests that more dramatic evolutionary events are likely responsible, such as a two-infall model (e.g. [Chiappini et al. 1997, 2001](#); [Romano et al. 2010](#); [Grisoni et al. 2017](#); [Noguchi 2018](#); [Spitoni et al. 2009, 2016, 2018, 2019, 2020](#)).

8 CONCLUSIONS

• We have modeled the Milky Way as a series of concentric annuli with $\Delta R_{\text{gal}} = 100$ pc width. We investigated a handful of assumptions about the SFH, the time-dependence of radial migration, and star formation efficiency, and a multitude of combinations thereof under a simulation-based model for stellar migration independent of free parameters.

• We found that similar numbers of star particles in h277 migrated inward as outward, and that the two proceed on different

timescales, indicating that they're potentially linked to different physical processes.

- We found that the e-folding timescales for star formation indicated by population averaged observations of Milky Way like galaxies are long (~ 15 Gyr in the solar annulus; Sánchez 2020).

- We found that our recipe for setting the gradients in both stellar surface density and metallicity yields the correct result. This is an indication that radial migration does not change the profile of these observed trends, only inducing scatter.

- We found that slightly different predictions in the stellar and gas-phase metallicity gradient are natural consequences of variations in the SFH.

- We found that different models for the SFH predicted different [O/Fe] gradients at the present day.

- We found that the time-dependence of radial migration indeed does have an impact on enrichment. Previous studies in the literature have assumed that this is not the case, due to the slow nature of migration (e.g. Minchev et al. 2013). However, we find that even for young stars, the tails of the present-day R_{gal} distribution are adequately long that when age-dependent migration is taken into account, the model predicts variations in the SN Ia rate that then impact predicted abundance ratios. We demonstrated that this is a means with which stellar migration may produce young, Fe-poor stars which can migrate to the solar annulus, and potentially be misinterpreted as young, α -rich stars. This is proof of concept that the radial migration of nucleosynthetic yields can proceed alongside the radial migration of stars, depending on which model for migration that you believe.

- These stars have been seen in observed data from APOGEE (e.g. Silva Aguirre et al. 2018). They postulate that since these stars have kinematics similar to the rest of the high- α population, that perhaps they are the consequence of stellar mergers or mass transfer events, producing truly old stars that simply appear to be younger. While these interpretations are not mutually exclusive, an observational test to ascertain the origins of the observed young α -rich population would have implications for which of the models for radial migration investigated here are the most realistic.

- In the observations, the high- α sequence is known to be most prominent at low R_{gal} and high $|z|$, and conversely, the low- α population at high R_{gal} and low $|z|$ (e.g. Hayden et al. 2015). We found that this is a natural consequence of stellar migration, though the detailed distributions depend on the SFH and the relative yields of α and iron-peak elements, both of which are highly uncertain, and we do not model them in detail here.

- We found that our inside-out model predicts an age-[α /Fe] relation which is in good agreement with the observed relation reported by Feuillet et al. (2019). Our recent starburst models predict a global α -enhancement that simply isn't seen in the data. This suggests that our current understanding of chemical evolution may be at odds with the findings of Mor et al. (2019) and Isern (2019) suggesting a recent factor of ~ 2 enhancement in the Milky Way SFH peaking ~ 2 Gyr ago.

- We find that where our inside-out SFH model fails to agree with the age-[O/Fe] relation reported by Feuillet et al. (2019), it tends to overpredict ages at a given [O/Fe]. However, it tends to fail in a manner such that the Feuillet et al. (2019) relation agrees with the stars that we would call Fe-poor - that is, the stars that are α -enhanced due to forming out of an Fe-poor ISM due to the same variations in the SN Ia rate that can produce young, α -rich stars.

While this may be coincidence, if we take the observations at face value, it would suggest that our model is overpredicting the rate of Fe injection, and that perhaps SN Ia yields of Fe should be lower. If we take the model at face value, it suggests that APOGEE+Gaia targets preferentially sample young, α -rich stars (Feuillet et al. 2019 used APOGEE data for stars with Gaia parallaxes).

- We found that the age-metallicity relation (AMR) in both [O/H] and [Fe/H] reported by Feuillet et al. (2019) is better fit by our late starburst models. This is at odds with the findings regarding the age-[O/Fe] relation, where the inside-out model agreed with the data much better than the starburst models. This is interesting, because different observables are favoring different models for the SFH, suggesting that something more complicated is going on.

- The starburst models agreeing with the observed AMR has more to do with the effect of dilution than the starburst itself. In trying to model the Milky Way, we might be able to have our cake and eat it too if there were dilution with no ensuing starburst. This could suggest some accretion event that was primarily HI gas that hasn't yet cooled to be available for star formation.

- Off the midplane, our model-predicted AMR overestimates ages relative to Feuillet et al. (2019), just like in the age-[O/Fe] relation. We speculate that this may be related to the Sagitarrius dwarf galaxy; it's important to remember that our model galaxy does not have the Milky Way's dynamical history, but h277's dynamical history. *Jon and I are looking into this, but as I understand it, what I've written next is in general true.* h277 did not have a Sagitarrius-like accretion event. Since Sagitarrius has made multiple pericentric passages nearly head-on with the Milky Way disk, it's possible that young stars were kinematically heated to high $|z|$, an effect that would not be present in h277 without such an event. This would decrease our model predicted median ages at these heights by directly adding more young stars, and potentially not having noticeable effect in the midplane due to the much larger number of stars there.

- We find that our models naturally reproduce the variations in the observed metallicity distribution functions (MDFs) with Galactocentric radius. At low R_{gal} , the mode abundance in both [O/H] and [Fe/H] is high, and conversely low at high R_{gal} . However, our predicted distributions are too narrow, where in the observations the low R_{gal} MDF is significantly skew-negative, and conversely skew-positive at high R_{gal} (Hayden et al. 2015). Also in the observed relation, the mode abundance at 3 - 5 kpc is strikingly similar to the mode abundance at 5 - 7 kpc. Our models fail to reproduce this, though it may be tied to a cessation of star formation in the inner galaxy as suggested by Peek (2009) and Fraternali & Tomassetti (2012).

- We find that none of our models predict a Milky Way-like dichotomy in [α /Fe], as observed by many studies. This suggests that inside-out galaxy growth combined with radial migration, even if a recent starburst is included, is not adequate to explain the observed dichotomy. This is at odds with Sharma et al. (2020), though we believe our study to be the more robust.

- VICE is publicly available and open-source. It can be installed via pip (<https://pypi.org/project/vice>). Documentation is available at <https://vice-astro.readthedocs.io>. Source code is hosted at <https://github.com/giganano/VICE.git>.

9 ACKNOWLEDGEMENTS

We are grateful to Diane Feuillet for sharing the data from Feuillet et al. (2018) and Feuillet et al. (2019) with us. There will be others added, depending on whether or not they go here or on the author's list. I'll also need to add the SDSS acknowledgements since we made use of APOGEE data.

10 DATA AVAILABILITY

In case anyone hasn't seen one of these Data Availability statements yet, this is now a requirement by MNRAS. It wasn't when I submitted my last paper, but was by the time we were finished with the referee report, so I wound up having to add one. They just want you to say if the data are available to the reader or not, and where/how they can get it if they are. VICE is open source software, and as such the source code for these simulations is publicly available.⁵ The source code which produces the outputs presented in this paper as well as the figures are included as secondary material in the GitHub repository. While the aggregate of all outputs analyzed in this paper are sufficiently large that it is not conducive to store them on GitHub, we provide instructions on how to run our simulations and variations thereof. All observational data appearing in this paper is publicly available, and is also included with the source code for our simulations and figures.

Appendices

A NORMALIZING A FIDUCIAL STAR FORMATION HISTORY

- Derive formula for normalizing an SFH given the time-dependence at a given radius $f(t|R_{\text{gal}})$ and the radial dependence of the desired surface density gradient at late times $g(R_{\text{gal}})$. Neither need be normalized.

$$\dot{\Sigma}_{\star}(R_{\text{gal}}, t) = \dot{\Sigma}_{\star,0}(R_{\text{gal}})f(t|R_{\text{gal}}) \quad (18)$$

$$\Sigma_{\star}(r) = \Sigma_{\star,0}g(R_{\text{gal}}) \quad (19)$$

- Integrate surface density of star formation with time and you get the present day surface density gradient at that radius. This yields the unknown $\dot{\Sigma}_{\star,0}$ in terms of $\Sigma_{\star}(R_{\text{gal}})$ and subsequently the unknown $\Sigma_{\star,0}$.

$$\Sigma_{\star}(R_{\text{gal}}) \approx (1-r) \int_0^T \dot{\Sigma}_{\star}(R_{\text{gal}}, t) dt \quad (20a)$$

$$= (1-r)\dot{\Sigma}_{\star,0}(R_{\text{gal}}) \int_0^T f(t|R_{\text{gal}}) dt \quad (20b)$$

$$\implies \dot{\Sigma}_{\star,0}(R_{\text{gal}}) = \Sigma_{\star}(R_{\text{gal}}) \left[(1-r) \int_0^T f(t|R_{\text{gal}}) dt \right]^{-1} \quad (20c)$$

$$= \Sigma_{\star,0}g(R_{\text{gal}}) \left[(1-r) \int_0^T f(t|R_{\text{gal}}) dt \right]^{-1} \quad (20d)$$

- Integrate surface density over area of the disk and you get the present day Milky Way stellar mass. This solves for the unknown $\Sigma_{\star,0}$:

$$M_{\star}^{\text{MW}} = \int_0^R \Sigma_{\star}(R_{\text{gal}}) 2\pi R_{\text{gal}} dR_{\text{gal}} \quad (21a)$$

$$= \Sigma_{\star,0} \int_0^R g(R_{\text{gal}}) 2\pi R_{\text{gal}} dR_{\text{gal}} \quad (21b)$$

$$\implies \Sigma_{\star,0} = M_{\star}^{\text{MW}} \left[\int_0^R g(R_{\text{gal}}) 2\pi R_{\text{gal}} dR_{\text{gal}} \right]^{-1} \quad (21c)$$

- Combine the last two equations into $\dot{\Sigma}_{\star}(R_{\text{gal}}, t)$ and obtain the following equation:

$$\dot{\Sigma}_{\star}(R_{\text{gal}}, t) = A f(t|R_{\text{gal}}) g(R_{\text{gal}}) \quad (22)$$

where

$$A = M_{\star}^{\text{MW}} \left[(1-r) \int_0^R g(R_{\text{gal}}) 2\pi R_{\text{gal}} dR_{\text{gal}} \int_0^T f(t|R_{\text{gal}}) dt \right]^{-1} \quad (23)$$

This result makes intuitive sense: $f(t|R_{\text{gal}})$ specifies the time-dependence of the SFH and $g(R_{\text{gal}})$ specifies the radial dependence by construction, and M_{\star}^{MW} sets the overall normalization.

- This recipe implicitly assumes that radial migration does not significantly alter the surface density profile, and we have demonstrated in § X that this is the case for the Galactocentric radii of interest in this paper. It introduces scatter, but does not alter the overall dependence. This recipe can be employed in disk galaxy models as long as this is not violated.

⁵ <https://pypi.org/project/vice>
<https://vice-astro.readthedocs.io>
<https://github.com/giganano/VICE.git>

B VARIATIONS IN STAR FORMATION EFFICIENCY

Eventually there will be an appendix demonstrating that our assumption about τ_\star in § 2.8 do not have an impact on our models.

REFERENCES

- Abolfathi B., et al., 2018, *ApJS*, **235**, 42
 Ahumada R., et al., 2020, *ApJS*, **249**, 3
 Andrews B. H., Weinberg D. H., Schönrich R., Johnson J. A., 2017, *ApJ*, **835**, 224
 Asplund M., Grevesse N., Sauval A. J., Scott P., 2009, *ARA&A*, **47**, 481
 Bigiel F., Leroy A., Walter F., Brinks E., de Blok W. J. G., Madore B., Thornley M. D., 2008, *AJ*, **136**, 2846
 Bigiel F., Leroy A., Walter F., Blitz L., Brinks E., de Blok W. J. G., Madore B., 2010, *AJ*, **140**, 1194
 Bird J. C., Loebman S. R., Weinberg D. H., Brooks A., Quinn T. R., Christensen C. R., 2020, arXiv e-prints, p. arXiv:2005.12948
 Bland-Hawthorn J., Gerhard O., 2016, *ARA&A*, **54**, 529
 Brooks A. M., Zolotov A., 2014, *ApJ*, **786**, 87
 Buck T., 2020, *MNRAS*, **491**, 5435
 Buck T., Obreja A., Macciò A. V., Minchev I., Dutton A. A., Ostriker J. P., 2020, *MNRAS*, **491**, 3461
 Chiappini C., Matteucci F., Gratton R., 1997, *ApJ*, **477**, 765
 Chiappini C., Matteucci F., Romano D., 2001, *ApJ*, **554**, 1044
 Christensen C., Quinn T., Governato F., Stilp A., Shen S., Wadsley J., 2012, *MNRAS*, **425**, 3058
 Clarke A. J., et al., 2019, *MNRAS*, **484**, 3476
 Cristallo S., et al., 2011, *ApJS*, **197**, 17
 Daflon S., Cunha K., de la Reza R., Holtzman J., Chiappini C., 2009, *AJ*, **138**, 1577
 Edvardsson B., Andersen J., Gustafsson B., Lambert D. L., Nissen P. E., Tomkin J., 1993, *A&A*, **500**, 391
 Feuillet D. K., et al., 2018, *Monthly Notices of the Royal Astronomical Society*, **477**, 2326
 Feuillet D. K., Frankel N., Lind K., Frinchaboy P. M., García-Hernández D. A., Lane R. R., Nitschelm C., Roman-Lopes A. r., 2019, *MNRAS*, **489**, 1742
 Fraternali F., Tomasetti M., 2012, *MNRAS*, **426**, 2166
 Frinchaboy P. M., et al., 2013, *ApJ*, **777**, L1
 Gaia Collaboration et al., 2018, *A&A*, **616**, A1
 García-Benito R., et al., 2017, *A&A*, **608**, A27
 García Pérez A. E., et al., 2016, *AJ*, **151**, 144
 González Delgado R. M., et al., 2014, *A&A*, **562**, A47
 Grand R. J. J., et al., 2017, *MNRAS*, **467**, 179
 Grand R. J. J., et al., 2018, *MNRAS*, **474**, 3629
 Grisoni V., Spitoni E., Matteucci F., Recio-Blanco A., de Laverny P., Hayden M., Mikolaitis Š., Worley C. C., 2017, *MNRAS*, **472**, 3637
 Gunn J. E., et al., 2006, *AJ*, **131**, 2332
 Hayden M. R., et al., 2014, *AJ*, **147**, 116
 Hayden M. R., et al., 2015, *ApJ*, **808**, 132
 Haywood M., 2008, *MNRAS*, **388**, 1175
 Holmberg J., Nordström B., Andersen J., 2007, *A&A*, **475**, 519
 Holtzman J. A., et al., 2015, *AJ*, **150**, 148
 Isern J., 2019, *ApJ*, **878**, L11
 Johnson J. W., Weinberg D. H., 2020, *MNRAS*, **498**, 1364
 Kalirai J. S., Hansen B. M. S., Kelson D. D., Reitzel D. B., Rich R. M., Richer H. B., 2008, *ApJ*, **676**, 594
 Kennicutt Robert C. J., 1998, *ApJ*, **498**, 541
 Kennicutt R. C., Evans N. J., 2012, *ARA&A*, **50**, 531
 Kroupa P., 2001, *MNRAS*, **322**, 231
 Krumholz M. R., Burkhardt B., Forbes J. C., Crocker R. M., 2018, *MNRAS*, **477**, 2716
 Leroy A. K., Walter F., Brinks E., Bigiel F., de Blok W. J. G., Madore B., Thornley M. D., 2008, *AJ*, **136**, 2782
 Leroy A. K., et al., 2013, *AJ*, **146**, 19
 Licquia T. C., Newman J. A., 2015, *ApJ*, **806**, 96
 Loebman S. R., Ivezić Ž., Quinn T. R., Governato F., Brooks A. M., Christensen C. R., Jurić M., 2012, *ApJ*, **758**, L23
 Loebman S. R., et al., 2014, *ApJ*, **794**, 151
 Majewski S. R., et al., 2017, *AJ*, **154**, 94
 Maoz D., Graur O., 2017, *ApJ*, **848**, 25
 Maoz D., Mannucci F., 2012, *Publ. Astron. Soc. Australia*, **29**, 447

- Martig M., et al., 2016, *MNRAS*, **456**, 3655
 Matteucci F., Francois P., 1989, *MNRAS*, **239**, 885
 Mészáros S., et al., 2012, *AJ*, **144**, 120
 Minchev I., Chiappini C., Martig M., 2013, *A&A*, **558**, A9
 Minchev I., Chiappini C., Martig M., 2014, *A&A*, **572**, A92
 Minchev I., Steinmetz M., Chiappini C., Martig M., Anders F., Matijevic G., de Jong R. S., 2017, *ApJ*, **834**, 27
 Mor R., Robin A. C., Figueras F., Roca-Fàbrega S., Luri X., 2019, *A&A*, **624**, L1
 Navarro J. F., Frenk C. S., White S. D. M., 1997, *ApJ*, **490**, 493
 Nidever D. L., et al., 2014, *ApJ*, **796**, 38
 Nidever D. L., et al., 2015, *AJ*, **150**, 173
 Noguchi M., 2018, *Nature*, **559**, 585
 Nordström B., Andersen J., Holmberg J., Jørgensen B. R., Mayor M., Pont F., 2004a, *Publ. Astron. Soc. Australia*, **21**, 129
 Nordström B., et al., 2004b, *A&A*, **418**, 989
 Peek J. E. G., 2009, *ApJ*, **698**, 1429
 Pinsonneault M. H., et al., 2014, *ApJS*, **215**, 19
 Recio-Blanco A., et al., 2014, *A&A*, **567**, A5
 Rojas-Arriagada A., et al., 2017, *A&A*, **601**, A140
 Romano D., Karakas A. I., Tosi M., Matteucci F., 2010, *A&A*, **522**, A32
 Roškar R., Debattista V. P., Stinson G. S., Quinn T. R., Kaufmann T., Wadsley J., 2008a, *ApJ*, **675**, L65
 Roškar R., Debattista V. P., Quinn T. R., Stinson G. S., Wadsley J., 2008b, *ApJ*, **684**, L79
 Salpeter E. E., 1955, *ApJ*, **121**, 161
 Sánchez S. F., 2020, *ARA&A*, **58**, 99
 Schmidt M., 1959, *ApJ*, **129**, 243
 Schmidt M., 1963, *ApJ*, **137**, 758
 Schönrich R., Binney J., 2009, *MNRAS*, **396**, 203
 Sellwood J. A., Binney J. J., 2002, *MNRAS*, **336**, 785
 Sharma S., Hayden M. R., Bland-Hawthorn J., 2020, arXiv e-prints, p. arXiv:2005.03646
 Shetrone M., et al., 2015, *ApJS*, **221**, 24
 Silva Aguirre V., et al., 2018, *MNRAS*, **475**, 5487
 Skrutskie M. F., et al., 2006, *AJ*, **131**, 1163
 Spitoni E., Matteucci F., Recchi S., Cescutti G., Pipino A., 2009, *A&A*, **504**, 87
 Spitoni E., Vincenzo F., Matteucci F., Romano D., 2016, *MNRAS*, **458**, 2541
 Spitoni E., Matteucci F., Jönsson H., Ryde N., Romano D., 2018, *A&A*, **612**, A16
 Spitoni E., Silva Aguirre V., Matteucci F., Calura F., Grisoni V., 2019, *A&A*, **623**, A60
 Spitoni E., Verma K., Silva Aguirre V., Calura F., 2020, *A&A*, **635**, A58
 Tacconi L. J., et al., 2018, *ApJ*, **853**, 179
 Vincenzo F., Kobayashi C., 2020, *MNRAS*, **496**, 80
 Wadsley J. W., Keller B. W., Quinn T. R., 2017, *MNRAS*, **471**, 2357
 Wang L., Dutton A. A., Stinson G. S., Macciò A. V., Penzo C., Kang X., Keller B. W., Wadsley J., 2015, *MNRAS*, **454**, 83
 Weinberg D. H., Andrews B. H., Freudenburg J., 2017, *ApJ*, **837**, 183
 Weinberg D. H., et al., 2019, *ApJ*, **874**, 102
 Wielen R., Fuchs B., Dettbarn C., 1996, *A&A*, **314**, 438
 Wilson J. C., et al., 2019, *PASP*, **131**, 055001
 Zamora O., et al., 2015, *AJ*, **149**, 181
 Zolotov A., et al., 2012, *ApJ*, **761**, 71